CHALMERS
UNIVERSITY OF TECHNOLOGY

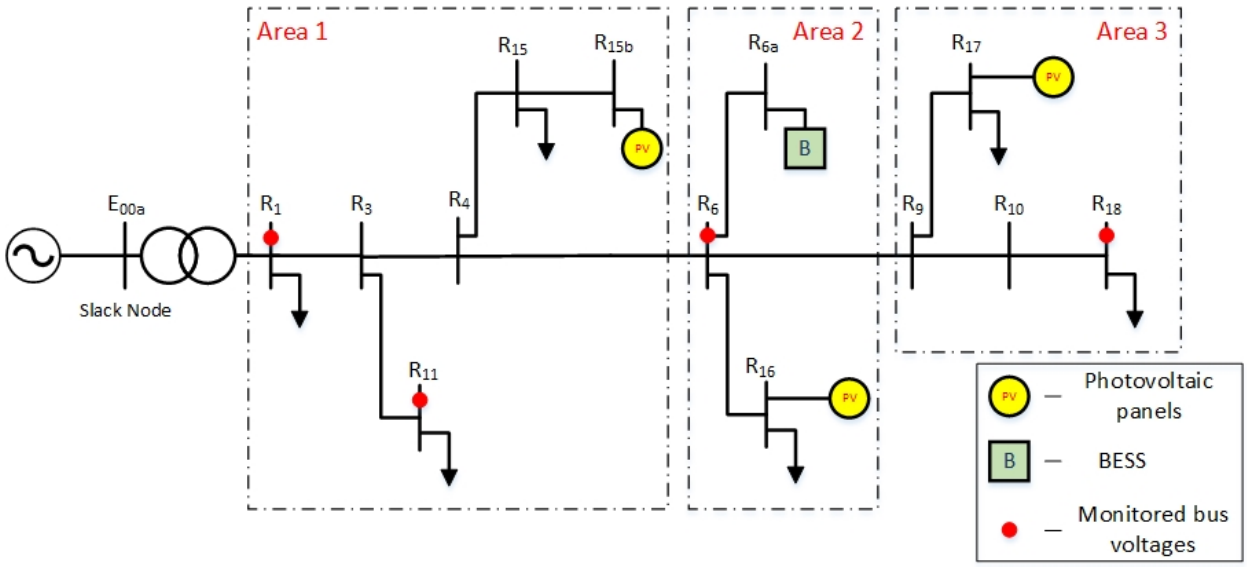

Coordinated voltage control in distribution systems using model predictive control strategies

Master's thesis in Electric Power Engineering

DEVGEET PATEL

Department of Electrical Engineering
CHALMERS UNIVERSITY OF TECHNOLOGY
Gothenburg, Sweden 2021

Master's Thesis 2021

Coordinated voltage control in distribution systems using model predictive control strategies

Devgeet Kamleshkumar Patel

CHALMERS
UNIVERSITY OF TECHNOLOGY

Department of Electrical Engineering
Division of Electric Power Engineering
Chalmers University of Technology
Gothenburg, Sweden 2021

Coordinated voltage control in distribution systems using model predictive control strategies
DEVGEET KAMLESHKUMAR PATEL

Supervisors:
David Steen, Department of Electrical Engineering
Ankur Srivastava, Department of Electrical Engineering
Examiner:
Le Anh Tuan, Department of Electrical Engineering

Master's Thesis 2021
Department of Electrical Engineering
Division of Electric Power Engineering
Chalmers University of Technology
SE-412 96 Gothenburg
Telephone +46 31 772 1000

Typeset in LaTeX
Printed by Chalmers Reproservice
Gothenburg, Sweden 2021

Coordinated voltage control in distribution systems using model predictive control strategies
DEVGEET KAMLESHKUMAR PATEL

Department of Electrical Engineering
Division of Electric Power Engineering
Chalmers University of Technology
Gothenburg, Sweden 2021

Abstract

The large scale integration of the distributed energy resources into the electric grid has increased multi-fold in the past few decades. With this large scale integration of the renewable energy resources into the distribution system, new challenges arise in operation, control and stability of the network. Due to the variable nature of the distributed energy resources, constant fluctuations in the voltage can be seen in the system. Model predictive control strategies can overcome the complex control problems in the distribution system with large scale integration of photo-voltaic, battery energy storage system and other loads providing demand response services. With model predictive control, it is possible to observe input and output constraints, set the objective function according to the requirements of the system operators and handle multi-variable control problems.

This thesis focuses on the description, implementation and comparison of 3 model predictive control based optimization strategies on a network with large amount of distributed energy resources. The modified CIGRÉ European LV residential network is considered as the test system in this thesis. Model predictive control based strategies studied in the thesis are centralized, decentralized and distributed. Distributed energy resources which are considered for the study are photovoltaics and battery energy storage systems which can be controlled with the power converter connected with the grid. These MPC based strategies are compared based on the utilization of the reactive power with the network and the simulation time for solving the model predictive control.

Case study results illustrates that the models developed for the centralized, decentralized and distributed model predictive control strategies act according to their respective design criteria. On the basis of the design criteria, it can also be seen that centralized and distributed control strategies are able to satisfactorily control bus voltages in the network while decentralized strategy fails to do so. The distributed control strategies utilise around 14% more reactive power reserves than the centralized model predictive control strategy.

A few scenarios were examined to study the impact on the network due to change in certain parameters of the model predictive controller. On changing the time-step, i.e. the time duration between which the control becomes active, it was seen that with smaller time-step value leads to faster action towards voltage recovery

but requires higher computational power. In another scenario where the number of measured voltage buses were changed, it was found that with higher number of those buses, reliability increase but at the cost of higher computational time. When the weights are varied for the control devices, it is seen that when higher weights are assigned, the contribution of that control device decreases and vice-versa.

Keywords: Backward-forward sweep power flow, battery energy storage, coordinated voltage control, distribution systems, model predictive control and photovoltaics

Acknowledgements

This thesis work has been conducted at the division of Electric Power Engineering, Department of Electrical Engineering at Chalmers University of Technology, Gothenburg, Sweden. I am very thankful to the department for providing me with this opportunity to work in my area of interest.

Firstly, I would like to express my sincere gratitude towards my supervisors Dr. David Steen and Ankur Srivastava for their continuous support, guidance and providing valuable feedback throughout the master thesis period. I am extremely thankful to my examiner Dr. Tuan Le for his encouragement and feedback towards the work. I would also like to specially thank Dr. Rabindra Mohanty for his valuable inputs and suggestion during the master thesis.

Finally, I would like to thank my family and friends for all the encouragement and support during the thesis.

Devgeet Kamleshkumar Patel, Gothenburg, January 2021

Contents

List of Figures xiii

List of Tables xv

List of abbreviations xvii

1 Introduction 1
- 1.1 Background and previous work . . . 1
- 1.2 Aim . . . 3
- 1.3 Thesis outline . . . 3

2 Theory 5
- 2.1 Battery energy storage system (BESS) . . . 5
- 2.2 Solar Photovoltaics . . . 6
- 2.3 Model Predictive Control . . . 6
  - 2.3.1 Overview . . . 6
- 2.4 Coordinated Voltage Control using MPC . . . 8
  - 2.4.1 Predictive Centralized Voltage Control (PCVC) . . . 9
  - 2.4.2 Predictive Decentralized Voltage Control (PDVC) . . . 10
  - 2.4.3 Sequential Predictive Distributed Voltage Controller (S-PDiVC) 12
  - 2.4.4 Parallel Predictive Distributed Voltage Controller (P-PDiVC) 14
- 2.5 Electric network systems . . . 16
- 2.6 Power flow for radial network . . . 17
  - 2.6.1 Backward-Forward Sweep Method . . . 17
    - 2.6.1.1 Basic algorithm . . . 17

3 Methods 21
- 3.1 The distribution system description . . . 21
- 3.2 PV and load profile . . . 21
- 3.3 The MPC controller . . . 22
- 3.4 MPC controller settings . . . 24
- 3.5 System simulation . . . 25

4 Results and discussion 27
- 4.1 No control . . . 28
- 4.2 PCVC strategy response . . . 30
- 4.3 PDVC strategy response . . . 33

4.4 S-PDiVC strategy response . . . 36
4.5 P-PDiVC strategy response . . . 39
4.6 Comparison of results of the MPC strategies . . . 42
4.7 Effect of various parameter on the MPC-based control . . . 43
4.7.1 Scenario 1: Effect of time-step of the measurement data . . . 43
4.7.1.1 Case 1: 5s time-step . . . 43
4.7.1.2 Case 2: 10s time-step . . . 44
4.7.1.3 Case 3: 20s time-step . . . 45
4.7.1.4 Scenario 1: Discussion . . . 47
4.7.2 Scenario 2: Selection of measured buses . . . 47
4.7.2.1 Case 1: Only 1 measured bus . . . 47
4.7.2.2 Case 2: 4 measured buses . . . 49
4.7.2.3 Case 3: All the buses in the network . . . 49
4.7.2.4 Scenario 2: Discussion . . . 50
4.7.3 Scenario 3: Effect of weights of the control devices . . . 51
4.7.3.1 Case 1: Low weight to R_{R15b} . . . 51
4.7.3.2 Case 2: Equal weight to R_{R15b} . . . 52
4.7.3.3 Case 3: High weight to R_{R15b} . . . 52
4.7.3.4 Scenario 3: Discussion . . . 53

5 Sustainability aspects **55**
5.1 Ecological aspect . . . 55
5.2 Social aspect . . . 55
5.3 Economical aspect . . . 55

6 Conclusion and future work **57**
6.1 Conclusions . . . 57
6.2 Future work . . . 58

Bibliography **59**

Appendix **I**

1 Appendix 1 **III**

List of Figures

1.1 Installed capacity of renewables around the world. Source: IRENA [2] 1

2.1 Solar PV attached to the AC grid 6
2.2 Basic concept of MPC reference 7
2.3 Tree diagram for different MPC methods 8
2.4 PCVC Architecture 9
2.5 PDVC Architecture 11
2.6 S-PDiVC Architecture 13
2.7 P-PDiVC Architecture 15
2.8 Radial system 16
2.9 Loop system 16
2.10 Network system 17

3.1 The modified CIGRÉ European LV residential network [28] 21
3.2 The PV and load profile 22
3.3 The PV and load profile with the measurement points data 26

4.1 The modified CIGRÉ test system 27
4.2 No control - Bus voltages in area 1 28
4.3 No control - Bus voltages in area 2 29
4.4 No control - Bus voltages in area 3 29
4.5 PCVC - Bus voltages in area 1 30
4.6 PCVC - Bus voltages in area 2 31
4.7 PCVC - Bus voltages in area 3 31
4.8 PCVC - Monitored bus voltages 32
4.9 PCVC - Reactive power used in all control buses 32
4.10 PDVC - Bus voltages in area 1 33
4.11 PDVC - Bus voltages in area 2 34
4.12 PDVC - Bus voltages in area 3 34
4.13 PDVC - Monitored bus voltages 35
4.14 PDVC - Reactive power used in all control buses 35
4.15 S-PDiVC - Bus voltages in area 1 36
4.16 S-PDiVC - Bus voltages in area 2 37
4.17 S-PDiVC - Bus voltages in area 3 37
4.18 S-PDiVC - Monitored bus voltages 38
4.19 S-PDiVC - Reactive power used in all control buses 38
4.20 P-PDiVC - Bus voltages in area 1 39

4.21 P-PDiVC - Bus voltages in area 2 40
4.22 P-PDiVC - Bus voltages in area 1 40
4.23 P-PDiVC - Monitored bus voltages 41
4.24 P-PDiVC - Reactive power used in all control buses 41
4.25 The PV and load profile with the measurement points data 44
4.26 The MPC response 44
4.27 The PV and load profile with the measurement points data 45
4.28 The MPC response 45
4.29 The PV and load profile with the measurement points data 46
4.30 The MPC response 46
4.31 Case 1.1: Measured bus: R_{11} 48
4.32 Case 1.2: Measured bus: R_6 48
4.33 Case 2: Measured bus: R_1, R_6, R_{11} and R_{18} 49
4.34 All network buses 50
4.35 Case 1: Very low weights to R_{15b} 52
4.36 Case 2: Equal weights to R_{15b} 52
4.37 Case 3: Very high weights to R_{15b} 53

List of Tables

4.1 Area wise division of buses 27
4.2 Comparison of different MPC strategies 42
4.3 Case wise summary for scenario 2 50
4.4 Case wise summary for scenario 3 53

1.1 Line data for the network in Figure 3.1 III

List of abbreviations

AC	Alternating Current
BESS	Battery Energy Storage System
BFS	Backward Forward Sweep
CVC	Coordinated Voltage Control
DC	Direct Current
DER	Distributed Energy Resource
DG	Distributed Generation
DSO	Distribution System Operator
LVC	Low Voltage Control
LV	Low Voltage
MPC	Model Predictive Control
MV	Medium Voltage
P-PDiVC	Parallel-Predictive Distributed Voltage Control
PCVC	Predictive Centralized Voltage Control
PDVC	Predictive Decentralized Voltage Control
PV	Photo-Voltaic
QP	Quadratic Programming
S-PDiVC	Sequential-Predictive Distributed Voltage Control
TSO	Transmission System Operator
VSC	Voltage Source Converter

1

Introduction

This chapter includes an overview of the background and motivations for the thesis work.

1.1 Background and previous work

There is a constant ongoing challenge with respect to the large scale integration of demand side distributed energy resources (DERs) like battery energy storage systems (BESS) and generation side DERs like photovolatic (PV) and wind resources. International Energy Agency (IEA) in [1], mentions that by 2024, there will be 50% increase in the renewable generation capacity compared to the year 2019. The total installed capacity of renewable energy resources around the world has more than doubled in the past 10 years can be seen in Figure 1.1. The renewable energy resources like geothermal, wind, solar and bio-fuel are included in the report [2]. Solar PVs provide around 15% and wind power provide around 20% of the total renewable-based installed capacity around the world.

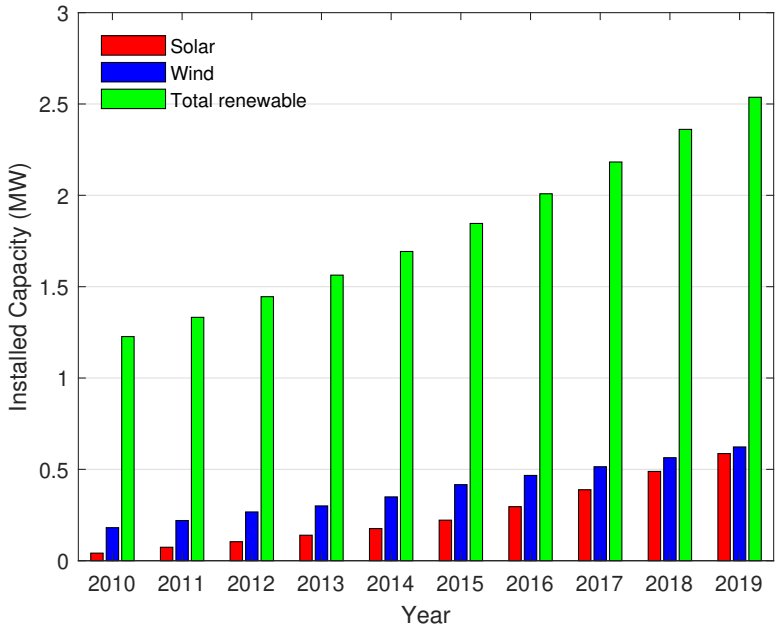

Figure 1.1: Installed capacity of renewables around the world. Source: IRENA [2]

With this large scale integration of the renewable energy resources into the system, new challenges arise in the operation and its control. Wind power is very difficult to control due to it's variable nature. This makes the wind power harder to control for the transmission system operators (TSO) as they need to actively manage power delivery to loads. This might lead to an increase in the cost for production and consumption balance and decrease the system reliability [3]. The gas turbines and hydro power being dispatchable in nature are easier to control. The solar PV and wind turbines interfaced with power converters has very low inertia. This causes a severe frequency and voltage stability problems if not controlled properly. One of the frequency problem called the '50.2 Hz problem' can be observed in Germany due to large number of existing PVs.

The problem with the large scale integration of the distributed generation leading to frequency and voltage instability can be dealt with by proper control of their output. The local voltage fluctuations can occur in the distribution system with high PV generation because of cloud effect [4]. Due to this constantly changing output of active power from DGs, the LV side consumers can see a frequent variations in voltage. The distribution system operators (DSO) do not have enough measurement data from LV side consumers and hence cannot act upon this voltage variations. This leads to DSO putting technical restrictions on the installed PVs to reduce the active power and provide reactive power compensation at a particular power factor for a better grid operation [5].

Having high penetration of distributed generation brings new challenges for the DSO with respect to voltage control performance in LV distribution systems as they are not designed to host generation locally [6], [7]. The high PV penetration in the system, considering the variable production based on the time of the day, cloud cover and the season poses problems in regulating the LV bus voltages effectively using common methods involving capacitor banks and tap-changing transformers at MV substations. For distribution systems with connected DGs like PV and BESS, grid codes can be added to impose restrictions on the DGs, to provide local voltage support[8].

Optimization based control methods can provide great advantages towards automating the coordination in the system. These methods could help the system having a large number of DGs connected to the system to automatically determine and change the ideal set point for each of the device rather than manually changing it. Another advantage is that it would be possible to define and implement a new objective and change the model to add new devices into the system and put more control variables for the optimization problem.

While developing an optimization-based coordinated control, many challenges are faced. The controller can be designed as a single, central optimizer handling the overall objective function of the system and determining the optimal set point changes to all the control devices. The central controller will give optimal results for the defined objective function taking into account all the control devices of the system but also faces drawbacks like lesser reliability of the system in case of the failure of the central controller; higher processing time since it considers all the control devices of the system leading to high complexity to implement practically. Another

choice can be multiple decentralized optimizers controlling only few devices in an area but with no knowledge of its interactions with other optimizers. Decentralized controllers can be easier to implement but they have a disadvantage of the loss of interaction information between the different areas. Another type of control being distributed control which has the architecture of the decentralized control and performance similar to the centralized controller as it takes the interaction between the optimizers into account [9].

In [10], the authors discusses local voltage control (LVC) methods to control active and reactive power output from PVs for effectively increasing the input capacity in the system. The authors have compared the existing commercially available methods to more advance commercially unavailable LVC techniques for the discussed scenario. For controlling active and reactive power from PVs, [11] introduces a central MPC based controller so that the voltage in MV distribution system with PVs remains in limits. In [7] and [12], the authors have proposed a single centralized controller which can control the set point values to the transformer tap changer's and DG's (wind power and PV) local controller. In [13], a few MPC strategies namely centralized, decentralized and distributed methods to control active power of a BESS are discussed. In [14], the author compares centralized, decentralized and distributed MPC-based voltage control methods in distribution system with PV and BESS. There is a need to compare various strategies discussed in above research for a distribution system with large-scale integration of PV and BESS which would be done in the thesis.

1.2 Aim

The thesis aims to investigate and compare voltage control strategies based on MPC framework which calculates the changes in the set point to local controllers of BESS and PV and thus optimally control the set point changes to local controllers of device. The controller algorithm will be simulated using MATLAB for different MPC based control strategies[15]. A total of three different MPC based strategies is simulated and compared in terms of reactive power usage and processing time for the algorithm. Also, some scenarios are discussed to study the effect of change in various parameters of the MPC strategies.

The outcome of this thesis incorporates valuable results and provide a coordinated controller capable to control the PV and BESS.

1.3 Thesis outline

The thesis report is organised as follows:

Chapter 2 describes the theory related to the distributed energy resources like photovoltaics and battery energy storage systems. This chapter also focuses on the overview of model predictive control along with the different types of electrical network systems and the backward-forward sweep power flow. Different coordinated voltage control strategies have also been discussed in detail.

Chapter 3 describes the methodology for implementing the model predictive control strategies. The model predictive controller is described in detail. The distribution power system network under consideration has been described in detail. Adding to this, all the parameters required for the MPC controller has been mentioned.

Chapter 4 analyses the results for **three** different model predictive control strategies for the system described in the previous chapter 3. A few scenarios have also been discussed in an attempt to understand the effect on the network due to various parameters in MPC controller.

Chapter 5 discusses the sustainability aspect of the study.

Chapter 6 concludes the report with suggestions and ideas for improvement in future work.

2
Theory

This chapter includes the description of different model predictive control (MPC) strategies for voltage control in LV distribution systems with battery energy storage systems (BESS) and photovoltaics (PV). Three different strategies namely centralized, decentralized and distributed MPC are discussed along with their advantages and disadvantages.

2.1 Battery energy storage system (BESS)

Batteries play an important role in our daily life for almost everyone and many electronic-based devices rely a lot on batteries. Based on the purpose of usage, the size and type of battery varies. Large applications like in households, BESS can be utilized to deal with the daily variations in generations from solar PVs. BESS works on the principle of storing the excess electrical energy generated from PV system into chemical energy and providing electrical energy when there is a deficit of PV generation. [16].

In future power grids where the renewable integration will be much higher than today, energy storage would be a big necessity to deal with the variable nature of renewable energy resources. One of the issues to be solved is how much of these renewable resources can be added before the system becomes too unbalanced. One of the possible solution could be to have an electric storage in the system. For example, solar energy produces it's maximum power during midday hours but the peak demand is not the highest in that period. In that case, the energy storage comes into picture. Excess energy during the midday can be stored and be utilized during the peak hours when the solar generation is not at it's peak (evening).

The demand and supply difference during the midday creates a problem as the power produced in the grid needs to be highly ramped up during the midday to meet the demand during the evening. These rapid changes due to the solar generation fluctuation is difficult for the system to handle. The base load power producer like coal and nuclear power are not economical to handle if they are to shut down during some period of the day and restarted during the evening hours. This is the one of the biggest challenge for implementing the renewable energy sources in the electrical system.

Pumped hydro has been the most utilised technology for storing electricity in the last century. In present times too, it is the most used technology with economical and technical advantage. It has a 99% market share in the energy storage. Battery

technology is relative new but the market is making efforts to utilise it more. The advantages of the battery technology is that it can be used on either side of the electric grid, i.e. demand and supply which makes it more flexible than pumped hydro. Increasing the battery storage in the system would grant larger quantity of renewable energy to be stored and also increase the reliability of the system [18]. Also, the BESS would require lesser area and won't have geographical restrictions as compared to pumper hydro.

Solar PVs coupled with energy storage can give a huge economic advantages. Solar energy could be stored when the prices are high and can be utilised when the prices are low. This not only gives the economic benefit but also help to stabilize the energy prices leading to lesser grid expansion costs [16].

2.2 Solar Photovoltaics

Solar photovoltaics (PV) is used to produce electricity from solar irradiation. It works on the principle of photoelectric effect. The photoelectric effect is the process in which electric current can be produced on exposure to light. Only certain materials have the tendency to do it and silicon is one of them. Most of the present day solar cells are made of silicon. Solar cells can be mounted on top of the buildings to serve as an energy resource for the nearby areas. The solar PV can be scaled based on the desired power by decreasing/ increasing the number of solar cells. The working principle for the solar PV attached to AC grid is shown in Figure 2.1. An inverter converts the DC power produced by the solar PV to AC which can be supplied to AC loads in the grid.

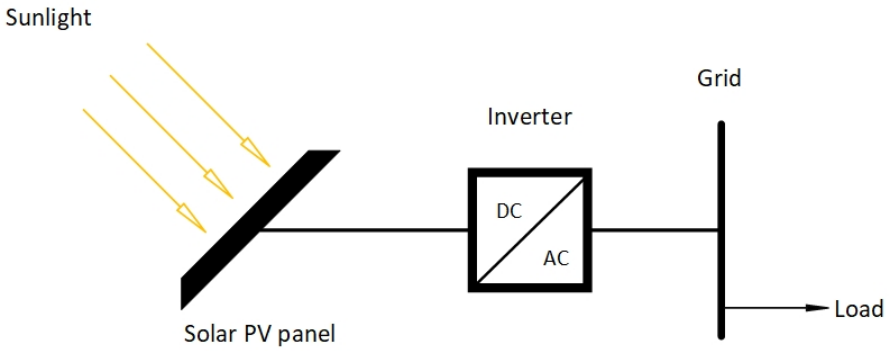

Figure 2.1: Solar PV attached to the AC grid

2.3 Model Predictive Control

2.3.1 Overview

An overview of MPC theory is explained in the current section. Choosing MPC has various advantages over other control methods. The most notable advantage of MPC is that it optimizes the current time slots, keeping the future time slots into

consideration. Using Model predictive control (MPC) can lead to a great opportunity to overcome the complex control problems in distribution systems with large number of photo-voltaic (PV), battery energy storage system (BESS) and other load providing demand response services. Implementing MPC in such power systems can offer many advantages like observing constraints on inputs and outputs, handling of multi-variable control problems, etc. The controllable devices needs to be controlled close to their physical limits in real time compared to conventional generators in the transmission networks which have higher power capacities. Cost-effectiveness of control actions would become vital if distribution system operators impose control requirements of these energy resources with the aim of deferring costly network reinforcements due to their integration.

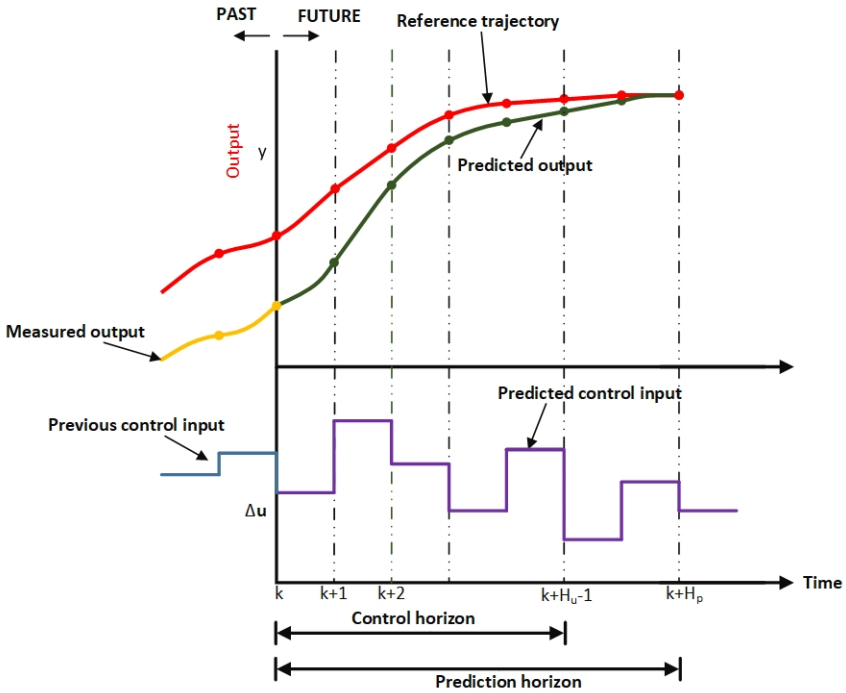

Figure 2.2: Basic concept of MPC reference

MPC finds a control action sequence over a control horizon H_u, taking into consideration the system response to these actions over the prediction horizon H_p based on the defined objective function [20]. Figure 2.2 describes the basic concept behind MPC. At any time instant k, controlled determines the predicted control trajectory using the most recent measurements available. With an aim to meet the required target trajecory $\boldsymbol{r}(k)$ for output $\boldsymbol{y}(k)$ by time $k + H_p$, a trajectory is obtained for the next $k + H_u$ - 1 time steps. Predictive control utilises the receding horizon idea. This means that at any time k, only the first control action $\Delta\mathbf{u}(k)$ is determined by the predictive controller. Once the above steps are performed, the internal clock of the controller is updated to time $k + 1$ with new measurement values available at that time. The states are updated based on the previous control action Δu(k) taken. The above process is then repeated for the next time step $k + 1$ in a similar way. The prediction horizon H_p should be selected such that the control actions are

accounted for over the next H_u time steps. This implies that the control horizon should be smaller than the prediction horizon, i.e., $H_p \geq H_u$.

In [14], the author has compared local voltage control (LVC) with other MPC models for distribution systems hosting large amounts of PV and BESS. The MPC models are described in detail in sections (2.4.1) - (2.4.4) below. The results in [14] indicate that MPC performs much better than the LVC in keeping the voltage in the limits. In [19], the author discusses a double time scaled coordinated MPC based voltage control where the system could operate at two different time scales, ie. fast-time scale control and slow-time scale control, based on the long term or short term action required. The benefit of this method is it's effective operation based on the type of device in consideration. But complex architecture and very fast action in fast time scale control mode leads to problems in computational speed.

2.4 Coordinated Voltage Control using MPC

Having high penetration of distributed generation brings new challenges to the DSO with respect to voltage control performance in LV distribution systems as they are not designed to utilise local generation [6], [7]. As monitoring of voltage on the LV side is uncommon in present times, DSO remains unaware of the changes in voltage occurring at the consumer side. The high PV penetration in the system, considering the variable production based on the time of the day, cloud cover and the season poses problems in regulating the LV bus voltages effectively using commonly available methods involving capacitor banks and tap-changing transformers at MV substations. The voltage can be controlled in a better way by increasing the voltage measurements and better communication in the system. Utilizing MPC helps to increase the capability of the controllers since future actions can be predicted.

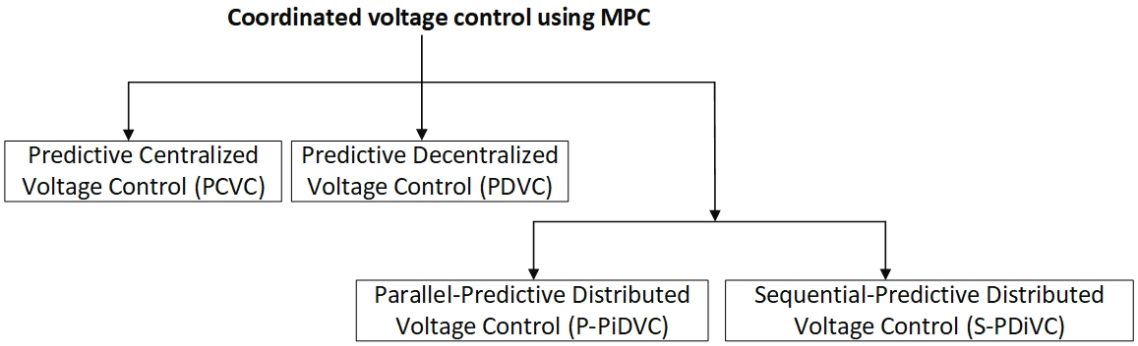

Figure 2.3: Tree diagram for different MPC methods

In the process of selecting the most suited control strategy, it is required to study the advantages and disadvantages of these strategies. Three different coordinated voltage control strategies namely centralized, decentralized and distributed MPC are described to select the best suited strategy to design for the thesis. Figure 2.3 shows a tree-diagram for the MPC methods explained below.

2.4.1 Predictive Centralized Voltage Control (PCVC)

The PCVC possesses a single optimizer which acts as a central model of the whole system. The PCVC takes in voltage measurement of all the monitored bus and control variables available as an input. There is a single objective function for the whole system. The architecture for PCVC is shown in Figure 2.4.

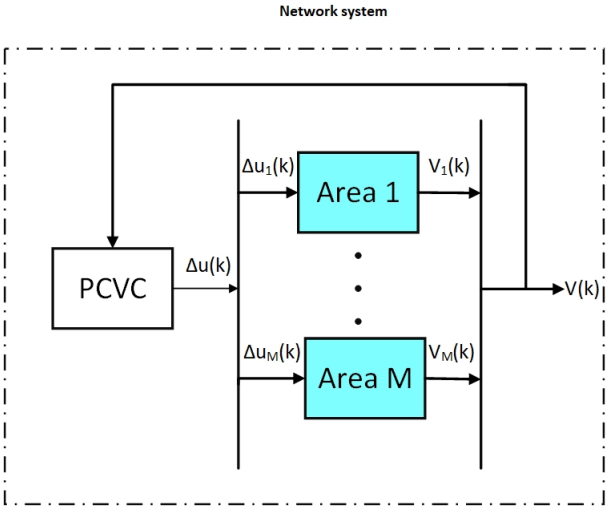

Figure 2.4: PCVC Architecture

At any time k, the PCVC optimizer takes the voltage measurement and control inputs k (denoted using $|k$ from now onwards) as inputs to the algorithm. The main objective of the PCVC optimizer is to minimize the control actions $\Delta u(k+i|k)$ over a duration of control horizon $i \in [0, H_u - 1]$. The setpoint change in control inputs, $u(k) = u(k - 1) + \Delta u(k)$ is sent to the controller by the optimizer, at each time step k. The objective function ϕ for PCVC can be expressed as a standard quadratic form as shown in (2.1). The constraints for the objective function can be described as in (2.2)-(2.6).

$$\phi = min \sum_{i=1}^{H_u-1} ||\Delta \boldsymbol{u}(k+i|k)||_R^2 + \sum_{i=1}^{H_p} \rho\epsilon(k+i|k) \tag{2.1}$$

Subject to,

$$\boldsymbol{V}(k+i+1|k) = \boldsymbol{V}(k+i|k) + \frac{\partial \boldsymbol{V}}{\partial \boldsymbol{u}} \triangle \boldsymbol{u}(k+i|k) \tag{2.2}$$

$$\boldsymbol{V}(k+i|k) \geq \boldsymbol{V}^{min}(k+i) - \epsilon_1(k+i|k) \tag{2.3}$$

$$\boldsymbol{V}(k+i|k) \leq \boldsymbol{V}^{max}(k+i) + \epsilon_2(k+i|k) \tag{2.4}$$

$$\boldsymbol{u}^{min}(k+i|k) \leq \boldsymbol{u}(k+i|k) \leq \boldsymbol{u}^{max}(k+i|k) \tag{2.5}$$

$$\triangle \boldsymbol{u}^{min} \leq \triangle \boldsymbol{u}(k+i|k) \leq \triangle \boldsymbol{u}^{max} \tag{2.6}$$

The PCVC should also deal with the cases where the optimization problem becomes infeasible. This can be solved with the help of a non-negative scalar slack variable $\epsilon(k + i|k)$. This slack variable $\epsilon(k + i|k)$ is penalized with a non-negative scalar parameter ρ [20].

Bus voltage evolution is predicted with the already available information at time k. An assumption has been made that the state information is available from the voltage measurement at any time instant k. A linearized state-space model of the power system is used to predict this evolution of bus voltages over the prediction horizon H_p. The state space model is obtained by linearization of the powerflow equations around the operating point. An updated voltage vector $\mathbf{V}(k+i+1)$ can be obtained by utilising the previous voltage vector $\mathbf{V}(k+i)$, reactive power changes and sensitivity gain $\frac{\partial \mathbf{V}}{\partial \mathbf{u}}$ as shown in (2.2).

The bus voltages are constrained to be within the minimum $\mathbf{V}^{min}(k+i)$ and maximum $\mathbf{V}^{max}(k+i)$ limits as shown in (2.3) and (2.4), respectively.

The control variables are selected as all the vectors of the reactive power set-points ($\mathbf{Q}_{\mathrm{b}}$) of BESS and vector of reactive power set-points of all PVs ($\mathbf{Q}_{\mathrm{pv}}$) in the network. At any time k, the change in control variables can be denoted as a vector $\mathbf{\Delta u}$.

$$\triangle \boldsymbol{u} = [\triangle \boldsymbol{Q_b^T}, \triangle \boldsymbol{Q_{pv}}^T]^T \tag{2.7}$$

The PCVC algorithm can be expressed as below:

1. For time instant k, the voltage measurements $\mathbf{V}$ for all monitored bus is received by the PCVC.
2. The optimal trajectory for the control variable is calculated by PCVC and it's first value u(k) is sent to the controllers.
3. Increment the time to $k + 1$, go to Step 1 and repeat the process.

2.4.2 Predictive Decentralized Voltage Control (PDVC)

PDVC strategy has same number of optimizers as there are areas in the electric system under consideration. If M number of areas are considered then there would be one PDVC optimizer for each area $j = [1, 2, ...,M]$.

The advantages of PDVC is that it is faster and the calculations by the optimizers are relatively independent from other areas. For an area j, communication is established between the optimizer and all the control devices available in area j. But since there is no communication between optimizers, each of them is unaware of the actions taken by other optimizers. This could lead to higher utilization of reactive power in certain areas than necessary, when there is significant interaction between different areas in the system. PDVC architecture is shown in Figure 2.5.

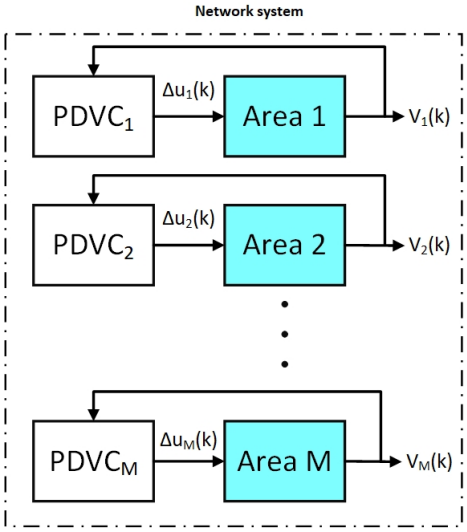

Figure 2.5: PDVC Architecture

For every area j, the PDVC optimizer objective function is expressed as ϕ_j. Each of the ϕ_j are independent from each other and consists of control variables ($\mathbf{u}_\mathrm{j}$), monitored bus voltages ($\mathbf{V}_\mathrm{j}$) and change in control variables (Δ $\mathbf{u}_\mathrm{j}$) of area j alone. The PDVC architecture avoids the interaction between $\mathbf{u}_\mathrm{j}$ in one area with the states in another areas. The PDVC mathematical model can be derived from the PCVC model. For each individual area j = [1, 2, ..., M], the objective function would be the copy of the PCVC objective function as shown in (2.1) with the constraints (2.2)-(2.6). The equations (2.2)-(2.6) can be reused for each area j individually and equivalent set of equations for a PDVC optimizer for area j can be obtained. The objective function ϕ_j of each PDVC optimizer is shown in 2.8.

$$\phi_j = min \sum_{i=1}^{H_u-1} ||\Delta \boldsymbol{u}_j(k+i|k)||_R^2 + \sum_{i=1}^{H_p} \rho\epsilon(k+i|k) \tag{2.8}$$

Subject to,

$$\boldsymbol{V}_j(k+i|k) \geq \boldsymbol{V}_j^{min}(k+i) - \epsilon_{1j}(k+i|k) \tag{2.9}$$

$$\boldsymbol{V}_j(k+i|k) \leq \boldsymbol{V}_j^{max}(k+i) + \epsilon_{2j}(k+i|k) \tag{2.10}$$

$$\boldsymbol{u}_j^{min}(k+i|k) \leq \boldsymbol{u}_j(k+i|k) \leq \boldsymbol{u}_j^{max}(k+i|k) \tag{2.11}$$

$$\triangle \boldsymbol{u}_j^{min} \leq \triangle \boldsymbol{u}_j(k+i|k) \leq \triangle \boldsymbol{u}_j^{max} \tag{2.12}$$

where the monitored bus voltages constraints are expressed in (2.9)-(2.10) and control variables constraints are expressed in (2.11)-(2.12). For each area, the voltage vector evolution can be expressed using (2.13).

$$\boldsymbol{V_j}(k+i+1|k) = \boldsymbol{V}_j(k+i|k) + \frac{\partial \boldsymbol{V_j}}{\partial \boldsymbol{u_j}} \triangle \boldsymbol{u_j}(k+i|k) \tag{2.13}$$

The PDVC optimizer control variables consists of all the reactive power set-points of BESS and reactive power set-points of PV in area j ∈ [1,M] as shown in (2.14)

$$\triangle \boldsymbol{u_j} = [\triangle \boldsymbol{Q_{bj}^T}, \triangle {\boldsymbol{Q_{pvj}}}^T]^T \tag{2.14}$$

For j ∈ [1,M], the PDVC_j algorithm can be expressed as below:

1. For time instant k, the voltage measurements $\mathbf{V}$ for all monitored bus in area j alone is received by the PDVC_j.
2. The optimal trajectory for the control variable is calculated by PDVC_j and it's first value $\text{u}_\text{j}(k)$ is sent to the local controllers.
3. Increment the time to $k + 1$, go to Step 1 and repeat the process.

2.4.3 Sequential Predictive Distributed Voltage Controller (S-PDiVC)

In this section, sequential distributed MPC (S-PDiVC) is described for the coordinated voltage control in the distribution system [21]. The architecture for this control strategy is shown in Figure 2.6.

In this strategy, there are as many optimizers as there are areas in the network. The optimizer in an area M has a communication with control devices of area M. Similar to PCVC, all the S-PDiVC optimizers receive the voltage measurements from all the monitored buses in the distribution system, at every time step k. S-PDiVC optimizers communicate with each other and each of the optimizer get the optimal input trajectories for all other optimizers for the current or previous time-step which depends on the position of the controller in the sequence, i.e j = [1, 2, ..., M]. For the current time step, S-PDiVC_1 communicates only with its nearest neighbor, S-PDiVC_2. Similarly, S-PDiVC_2 communicates only with it's neighbour S-PDiVC_3 and so on. Figure 2.6 also mentions that each of the optimizer receive the optimal control trajectories of all the optimizers which are before it in the sequence.

The S-PDiVC mathematical model can be obtained from PCVC model [22]. The S-PDiVC strategy for the voltage control can be formulated as below. The PCVC equations (2.1)-(2.6) can be altered for each of the area $j \in [1, M]$ and equivalent set of equations can be obtained for the S-PDiVC control. The objective function of each S-PDiVC ϕ_j is same as the objective function of PCVC case and can be written as (2.15).

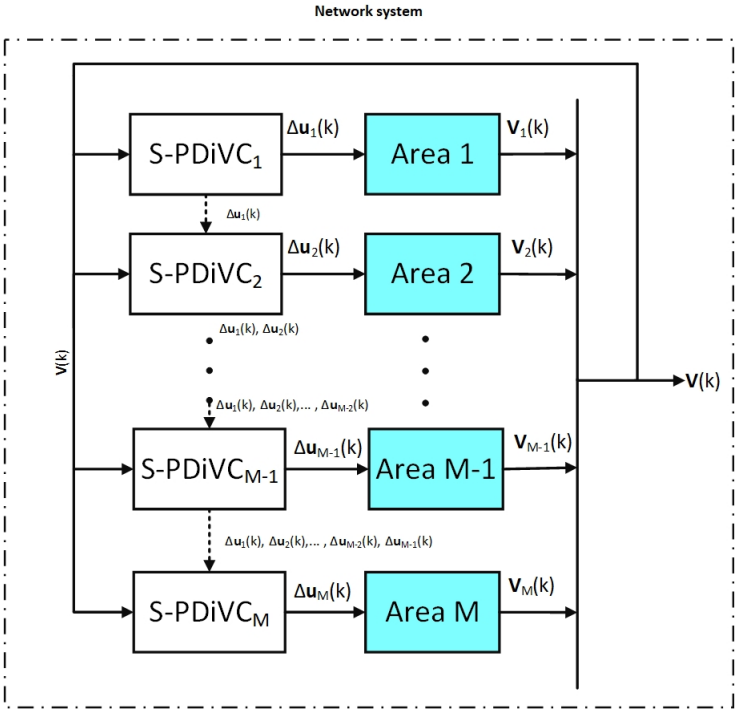

Figure 2.6: S-PDiVC Architecture

$$\phi_j = min \sum_{i=1}^{H_u-1} ||\Delta \boldsymbol{u}_j(k+i|k)||^2_{\tau_j R_j} + \sum_{i=1}^{H_p} \rho\epsilon(k+i|k) \tag{2.15}$$

The objective function in (2.15) has the constraints defined on the monitored bus voltages (2.16)-(2.17) and on control variables (2.18)-(2.19)

$$\boldsymbol{V}(k+i|k) \geq \boldsymbol{V}^{min}(k+i) - \epsilon_1(k+i|k) \tag{2.16}$$

$$\boldsymbol{V}(k+i|k) \leq \boldsymbol{V}^{max}(k+i) + \epsilon_2(k+i|k) \tag{2.17}$$

$$\boldsymbol{u}_j^{min}(k+i|k) \leq \boldsymbol{u}_j(k+i|k) \leq \boldsymbol{u}_j^{max}(k+i|k) \tag{2.18}$$

$$\triangle \boldsymbol{u}_j^{min} \leq \triangle \boldsymbol{u}_j(k+i|k) \leq \triangle \boldsymbol{u}_j^{max} \tag{2.19}$$

The control variables of S-PDiVC is similar to PDVC consisting of all the Q of BESS and Q of PV in area j as shown in (2.14). The evolution of voltage vector over time can be expressed using (2.20) for every $j \in [1,\ M]$.

$$\begin{aligned} \boldsymbol{V}(k+i+1|k) =& \boldsymbol{V}(k+i|k) + \frac{\partial \boldsymbol{V}}{\partial \boldsymbol{u_j}} \triangle \boldsymbol{u_j}(k+i|k) + \sum_{l=1, l\neq j}^{j-1} \frac{\partial \boldsymbol{V}}{\partial \boldsymbol{u_l}} \triangle \boldsymbol{u_l}(k+i|k) \\ &+ \sum_{l=j+1, l\neq j}^{M} \frac{\partial \boldsymbol{V}}{\partial \boldsymbol{u_l}} \triangle \boldsymbol{u_l}(k+i|k-1) \end{aligned} \tag{2.20}$$

τ is a vector which denotes the relative weights of all S-PDiVC optimizers in the distribution system. Relative weights for each area j is denoted by τ_j, hence $\tau = [\tau_1, \tau_2, ..., \tau_j, ..., \tau_M]$. For all $l \neq j$, the input to S-PDiVC$_\mathrm{j}$ is $\boldsymbol{u_l}$. The S-PDiVC algorithm can be expressed as below:

1. For time instant k, the voltage measurements $\mathbf{V}$ for all monitored bus in the network is received by all S-PDiVC optimizers.
2. For j $\in$ [1, M]
   (a) S-PDiVC$_\mathrm{j}$ receives the control variable trajectories $\Delta\mathbf{u}_\mathrm{l}(k+i)\ \forall\ l \in [j+1, ..., M]$, $l \neq j$ calculated at time k - 1. $i \in [0, 1, ..., H_u - 1]$
   (b) S-PDiVC$_\mathrm{j}$ also obtains the control variable trajectories $\Delta\mathbf{u}_\mathrm{l}(k+i)\ \forall\ l \in [1, ..., j-1]$, $l \neq j$ calculated at time k. $i \in [0, 1, ..., H_u - 1]$
   (c) The optimal trajectory for the control variable is calculated by S-PDiVC$_\mathrm{j}$ and it's first value $\mathrm{u_j}(k)$ is sent to the local controllers.
3. Increment the time to $k + 1$, go to step 1 and repeat the process.

2.4.4 Parallel Predictive Distributed Voltage Controller (P-PDiVC)

This section refers to an iterative cooperative distributed MPC. It is also referred to as P-PDiVC. The architecture is similar to that of PDVC. P-PDiVC consists of as many optimizers as there are subsystems/areas in the network. The advantage of the architecture is that it has relatively independent calculations by the optimizers and is faster but the downside being more complex infrastructure for communication. The P-PDiVC architecture is described in Figure 2.7. P-PDiVC shares similarities with the PCVC architecture. The objective function for P-PDiVC is a part of PCVC objective function. The P-PDiVC optimizers get voltage measurements from all monitored buses at every optimization time step k. Also, there is communication between optimizers- unlike S-PDiVC, all the P-PDiVC optimizers get the trajectory of optimal input of all the other P-PDiVC optimizers from the previous time step.

The mathematical model for the P-PDiVC is derived from the PCVC model [22]. P-PDiVC strategy can be applied for the voltage control in an LV distribution system. Considering there are M areas in the LV distribution system, the following formulation can be used for a P-PDiVC controller in every area $j \in$ [1, M]. The objective function of PCVC (2.21) and it's constraint equations (2.22) - (2.25) can be used for every area j and set of equations similar to PDVC case can be obtained for P-PDiVC. The objective function of each P-PDiVC ϕ_j is same as the global objective function of PCVC case and can be written as 2.21.

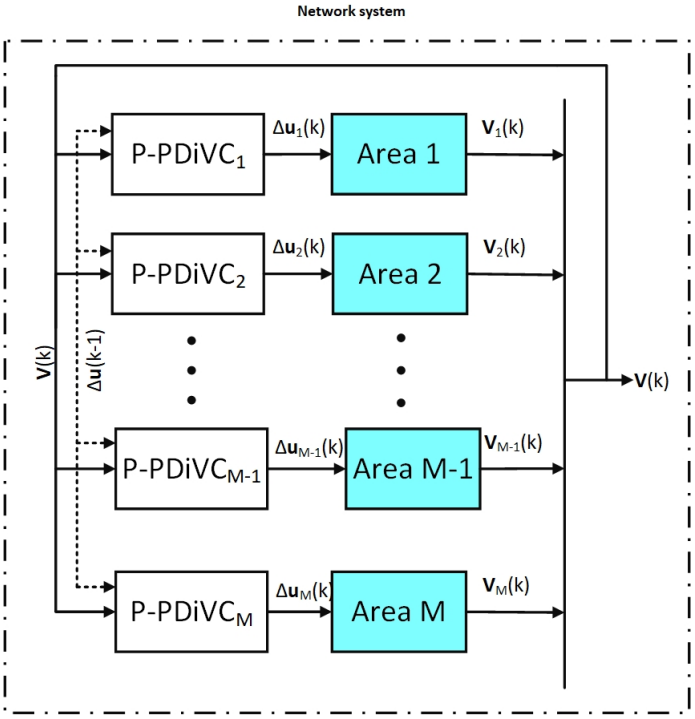

Figure 2.7: P-PDiVC Architecture

$$\phi_j = min \sum_{i=1}^{H_u-1} ||\Delta \boldsymbol{u}_j(k+i|k)||^2_{\tau_j R_j} + \sum_{i=1}^{H_p} \rho\epsilon(k+i|k) \tag{2.21}$$

The objective function 2.21 has the constraints on the monitored bus voltages and on control variables

$$\boldsymbol{V_j}(k+i|k) \geq \boldsymbol{V_j}^{min}(k+i) - \epsilon_{1j}(k+i|k) \tag{2.22}$$

$$\boldsymbol{V_j}(k+i|k) \leq \boldsymbol{V_j}^{max}(k+i) + \epsilon_{2j}(k+i|k) \tag{2.23}$$

$$\boldsymbol{u}_j^{min}(k+i|k) \leq \boldsymbol{u}_j(k+i|k) \leq \boldsymbol{u}_j^{max}(k+i|k) \tag{2.24}$$

$$\triangle \boldsymbol{u}_j^{min} \leq \triangle \boldsymbol{u}_j(k+i|k) \leq \triangle \boldsymbol{u}_j^{max} \tag{2.25}$$

The control variables of P-PDiVC is similar to PDVC consisting of all the ,Q of BESS and Q of PV in area j as shown in (2.14). The evolution of voltage vector over time can be expressed using (2.26) for every j = 1, 2,..., M.

$$\boldsymbol{V_j}(k+i+1|k) = \boldsymbol{V}_j(k+i|k) + \frac{\partial \boldsymbol{V_j}}{\partial \boldsymbol{u_j}} \triangle \boldsymbol{u_j}(k+i|k) + \sum_{l=1, l\neq j}^{i=M} \frac{\partial \boldsymbol{V}}{\partial \boldsymbol{u_l}} \triangle \boldsymbol{u_l}(k+i|k-1) \tag{2.26}$$

For each area j, the P-PDiVC takes in $\boldsymbol{u_l}$ $\forall l \neq j$ as an input and can be expressed as in (2.26). P-PDiVC algorithm follows the below steps:

1. For time instant k, the voltage measurements $\mathbf{V}$ for all monitored bus in the network is received by all P-PDiVC.
2. For $j = 1$ to M
   (a) P-PDiVC$_j$ receives the control variable trajectories $\Delta\mathbf{u}_l(k+i)\ \forall\ l \in [1,...,M]$, $l \neq j$ calculated at time k - 1. $i \in [0,1,...,H_u - 1]$
   (b) The optimal trajectory for the control variable is calculated by P-PDiVC$_j$ and it's first value $\boldsymbol{u_j}$(k) is sent to the local controllers. The trajectory $\boldsymbol{u_j}(k+i)$, $\forall i = [0,\ ...,H_u$ - 1] is sent to all other P-PDiVC optimizers l $\in$ [1,M], l $\neq$ j.
3. Increment the time to $k + 1$, go to step 1 and repeat.

2.5 Electric network systems

Distribution system are defined by three types namely radial system, loop system and network system. In sparsely populated areas, the radial distribution system is used. Radial systems are also cheapest to built.

A radial system consists of a single power source for a group of customers. In case of a power outage, power would be interrupted in the entire line which should be fixed before the system can be brought back to normal. Figure 2.8 shows a general diagram for a radial network.

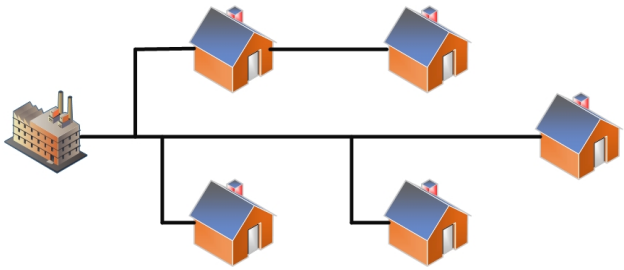

Figure 2.8: Radial system

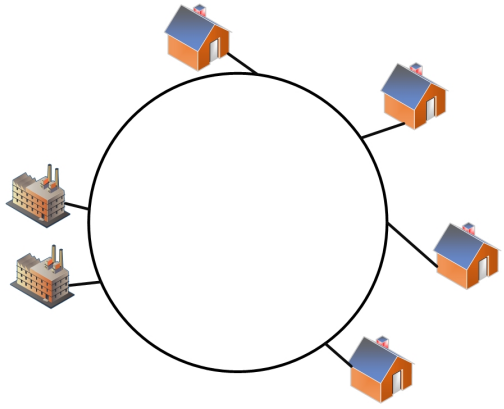

Figure 2.9: Loop system

The loop system, as the name suggests, loops through the desired area and returns to the starting point. This type of network is generally has an alternate power

source attached to it. With proper placing of switches power can be supplied to the customers from either direction. If one of the power source fails, switches are turned on or off automatically/ manually which can help retain the power in system. Figure 2.9 shows a general diagram for a loop network.

Network systems has more complex design compared to radial and loop networks. Network systems are interlocking loop systems. In this type of network, it is possible to feed the customer from two, or more different power sources. The system becomes more reliable due to this but it becomes more expensive. Due to this, it is used in dense and congested areas with high amount of loads. Figure 2.10 shows a general diagram for a network network

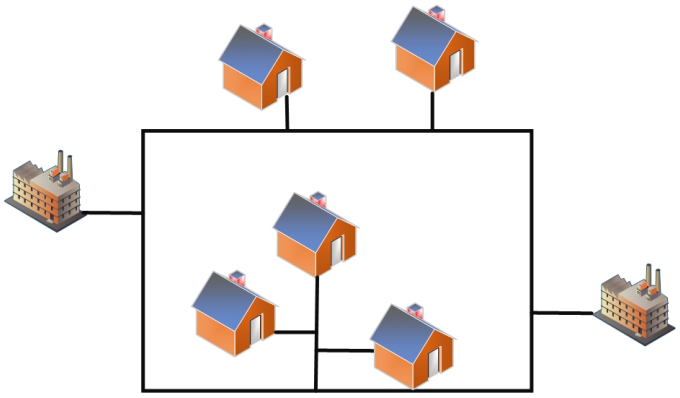

Figure 2.10: Network system

2.6 Power flow for radial network

The network system dealt with in this thesis is a radial network system hence only the suitable power flow algorithm is discussed in detail here.

2.6.1 Backward-Forward Sweep Method

Backward-Forward Sweep (BFS) method is used for highly radial distribution networks. The solution for the power flow is obtained by iterative solution from two sets of recursive equations [25]. The full description of the BFS method is explained in [26]. The BFS method can deal with various modeling challenges like sparse generation (PV nodes) and unbalanced loads. Simultaneously it has a high execution speed necessary for real-time application in power systems.

2.6.1.1 Basic algorithm

In BFS method can be solved in two separate ways by with and without consideration of P-V nodes in the distribution system[26].

1. *Without PV nodes in the system*: In this method, all the nodes other than the slack node are considered to be PQ nodes. Slack node voltage is kept constant and a flat start is assumed for all other nodes. For the i^{th} iteration, following steps are performed:

(a) Current injection calculation at k^{th} node:

$$C_k^{(i)} = \left[\frac{S(k)}{V_k^{(i-1)}}\right]^* - Y_k V_k^{(i-1)} \forall k = 1, 2, ..., n \tag{2.27}$$

where S_k and Y_k are the apparent power injected and the sum of shunt element admittances at k^{th} node. $V_k^{(i-1)}$ is the k^{th} node voltage for the (i-1)th iteration.

(b) Branch current calculation. The calculation is started from the branch connected at the end node and proceeding backwards. The calculation for the current at j^{th} branch is done as follows:

$$I_j^{(i)} = C_N^{(i)} + \sum_{f=1}^{T} I_f^{(i)} \forall j = br, , ..., 2, 1. \tag{2.28}$$

where C_N^i is the load current at N$_{th}$ node and T is the total branches from node N.

(c) Updating the voltages at nodes beginning from the slack node and proceeding towards the end node. The voltage at N^{th} node can be expressed as:

$$V_N^{(i)} = V_M^{(i)} - Z_j I_j^{(i)} \forall j = 1, 2, ..., br. \tag{2.29}$$

where Z_j represents the branch j impedance.

The above steps are iteratively solved until the convergence criteria is met.

2. *With PV nodes in the system*: In this method, the load nodes are treated as PQ nodes while the generator nodes are treated as PV nodes. Let us assume that there are q P-V nodes in the network, then for jth iteration, the procedure for correction of voltage magnitude is as follows:

(a) Calculate mismatch in voltage magnitude in all P-V nodes:

$$\nabla V_k^{(j)} = |V_k^{(sp)}| - |V_k^{(j)}| \qquad \forall k = 1, 2, ..., q \tag{2.30}$$

where, $V_k^{(sp)}$ is the specified voltage value at node k.

(b) Reactive current injection is calculated as follows:

$$\nabla I_Q^{(j)} = Z^{-1}[\nabla V]^{(j)} \tag{2.31}$$

where, Z is the real and constant impedance matrix with size as number of P-V nodes. The injected reactive current at k^{th} node can be computed as follows:

$$I_{kQ}^{(j)} = j|I_{kQ}^{(j)}| \tag{2.32}$$

(c) The total reactive power requirement Q_{kR} calculation, for all P-V nodes:

$$\begin{aligned} Q_{kR}^{(j)} &= Q_k^{(j)} + Q_{kL} \\ Q_k^{(j)} &= Im[V_k I_{kQ}'^*] \qquad \forall k = 1, 2, ..., n, \end{aligned} \tag{2.33}$$

where, Q_{kL} refers to the reactive power load at k^{th} node and I'_{kQ} is the sum of the required reactive current injection and the load current injection $= I_{kQ}^{(j)} + QI_{kL}$

(d) Check for all nodes whether calculated Q_{kR} $(= Q_{inj})$ corresponding to P_{inj} , satisfies the constraint given by $P_{inj}^2 + Q_{inj}^2 \leq S_{rated}^2$, where S_{rated} is the rated capacity for the PV inverter. If the constraint is not satisfied then a new P_{inj} and the corresponding Q_{inj} should be computed. To do this computation more effectively, a curve-fitting method is used to express Q_{inj} as a function of P_{inj} (for a fixed system topology). Curvefitting is a method for expressing a mathematical function which best fit to a series of data points. Here, P_{inj} and Q_{inj} are the data points. This method helps in avoiding the iterative process to find the new value of Q_{inj}.

These steps are performed iteratively until the voltage mismatches for all P-V nodes reaches below the tolerance limit.

3
Methods

3.1 The distribution system description

The single line diagram for of the modified CIGRÉ's European low voltage (LV) distribution network [27] is shown in Figure 3.1. The network is modified to represent the residential part of the network. The LV network is connected to the external grid through a 20/0.4KV, 400KVA transformer.

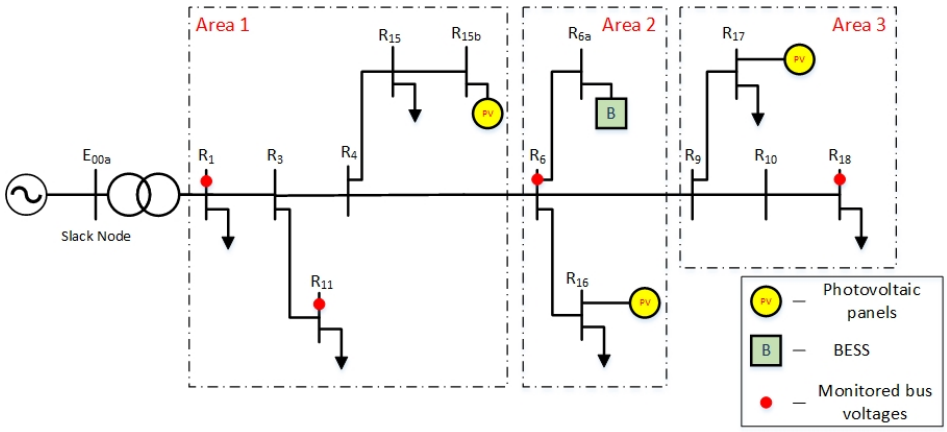

Figure 3.1: The modified CIGRÉ European LV residential network [28]

The network consists of 14 buses, 3 solar photovoltaics and 1 BESS. The solar PVs are located at buses R_{15b}, R_{16} and R_{17}, and the BESS is located at R_{6a}. The converters are located at all PVs and BESS and are assumed to be available for the voltage control of the network. Loads can be found at buses R_1, R_{11}, R_{15}, R_{16}, R_{17} and R_{18}. Bus R_{E00a} is considered as the slack bus. The constant power model is used for the network loads in order to get the true response of the MPC controller. The load profile is shown in the next section. The network data is shown in Appendix 1.

3.2 PV and load profile

In this section a PV profile and the load profile are described. Each solar PV has a rated capacity of 8KW. The PV data is measured every 0.2s. The PV profile for one of the solar PVs is shown in Figure 3.2a. The loads are treated as a constant power type, hence the power factor would be constant for all loads and is taken as 0.85 lagging. The load profile is shown in Figure 3.2b

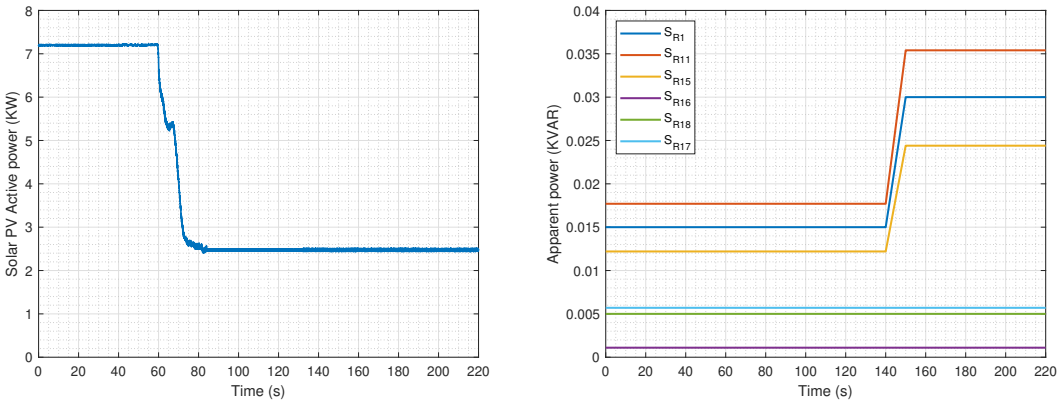

(a) The PV profile a solar PV **(b)** The load profile for all buses [KVAR]

Figure 3.2: The PV and load profile

3.3 The MPC controller

In MPC, a desired objective function with the available set of constraints can be optimized by finding a sequence of control action over the selected control horizon H_u, keeping in mind the response of the system model for a prediction horizon H_p [29]. For any time k, the controller uses the latest available voltage measurements at the remote buses to calculate the sequence of the reactive power output for the next H_u control time steps to get the remote bus voltages within the acceptable limits before the prediction horizon $k + H_p$. The predictive control model utilises the receding horizon principle and hence only the first control action $\Delta u(k)$ is considered for the control for the time step $k + 1$. The calculated $\Delta u(k)$ is sent to the local reactive power controllers at the PVs and BESS. Once the control action is performed, the MPC's clock is updated to $k + 1$ and with the remote bus measurements available at that instance, the process is repeated as mentioned for time step k. The main objective of the optimizer is to minimize the control actions $\Delta u(k+i|k)$ for the control horizon $i \in [0,\ H_u\ -\ 1]$. The set-point change can be expressed as $u(k) = u(k-1) + \Delta u(k)$.

A discretized state-space linear model of the power system is used for the predictive voltage controller. The states for the models are the remote bus voltage measurements and the inputs to the model are change in the reactive power output from the VSC. The given voltage at remote bus at time k would be denoted as "$|k$" from now on. The model shows how the voltage V(k + 1) at time k + 1 is calculated with the changes in the $\Delta u(k)$, the reactive power output from the VSC at time k depending on the sensitivity gain $\frac{\partial V}{\partial u}$. The sensitivity gain $\frac{\partial V}{\partial u}$ can be obtained by doing on-site step-response tests or from static power flow solution. For this model, it is calculated from the static power flow solution at each time step k. The state space model can be expressed as (3.1).

$$V(k+1) = V(k) + \frac{\partial V}{\partial u}\Delta u(k) \tag{3.1}$$

Using model stated in (3.1), it is possible to predict the evolution of the voltages for the next H_p time steps considering that the change in reactive power happens over the next H_u time steps. This model is expressed using (3.2).

$$\begin{bmatrix} V(k+1|k) \\ V(k+2|k) \\ V(k+3|k) \\ . \\ . \\ . \\ V(k+H_p|k) \end{bmatrix} = V(k) + \frac{\partial V}{\partial u} \begin{bmatrix} \Delta u(k|k) \\ \Delta u(k+1|k) \\ \Delta u(k+2|k) \\ . \\ . \\ . \\ \Delta u(k+H_u-1|k) \end{bmatrix} \tag{3.2}$$

The $\frac{\partial V}{\partial u}$ can be expressed according to (3.3) which shows that how the voltages at the remote bus is affected at different time steps based on the control action taken during previous time steps.

$$\frac{\partial \mathbf{V}}{\partial \mathbf{u}} = \begin{bmatrix} \frac{\partial V}{\partial u} & 0 & 0 & \cdots & 0 \\ \frac{\partial V}{\partial u} & \frac{\partial V}{\partial u} & 0 & \cdots & 0 \\ \frac{\partial V}{\partial u} & \frac{\partial V}{\partial u} & \frac{\partial V}{\partial u} & \cdots & 0 \\ \vdots & \vdots & \vdots & \ddots & \vdots \\ \frac{\partial V}{\partial u} & \frac{\partial V}{\partial u} & \frac{\partial V}{\partial u} & \cdots & \frac{\partial V}{\partial u} \\ \frac{\partial V}{\partial u} & \frac{\partial V}{\partial u} & \frac{\partial V}{\partial u} & \cdots & \frac{\partial V}{\partial u} \\ \vdots & \vdots & \vdots & \vdots & \vdots \\ \frac{\partial V}{\partial u} & \frac{\partial V}{\partial u} & \frac{\partial V}{\partial u} & \cdots & \frac{\partial V}{\partial u} \end{bmatrix} \tag{3.3}$$

The model is considered to be a single input-single output system and hence in the sensitivity gain matrix $\frac{\partial \mathbf{V}}{\partial \mathbf{u}}$ in (3.3), the non zero elements are considered to be the same. The controller objective function can be defined as in (3.4), which requires to solve the MPC problem by utilizing the least amount of change in the control inputs Δu with the available remote bus voltage measurements.

$$\phi = \min_{\Delta u} \sum_{i=0}^{H_u-1} \Delta u(k+i|k)^2 \tag{3.4}$$

The objective function ϕ in (3.4) is subject to the minimum and maximum constraints over the reactive power output from the VSC. The changes in the reactive power output from VSC are also contrainted to its minimum and maximum values. Both the constraints are valid for all values for $i \in [0,\, H_u - 1]$ as shown in (3.5) and (3.6) respectively.

$$u^{min} \leq u(k+i|k) \leq u^{max} \tag{3.5}$$

$$\Delta u^{min} \leq \Delta u(k+i|k) \leq \Delta u^{max} \tag{3.6}$$

The objective function ϕ in (3.4) is also subject to the minimum and maximum constraints over the remote bus voltages for all $i \in [1,\, H_p]$ as shown in 3.7.

$$V^{min} \leq V(k+i|k) \leq V^{max} \tag{3.7}$$

In some situations, it might happen that the reactive power limits are reached and might lead to the optimization problem being infeasible. In such critical situation, it should be made sure that the MPC controller provides the best solution, even though the voltage constraints are violated. To be able to achieve this, relaxation in voltage is considered and it is done by adding a linear penalty on maximum number of bus voltages violations (∞-norm). This penalty can be levied upon by introducing non negative scalar slack variables $\epsilon_1(k+i|k)$ and $\epsilon_2(k+i|k)$ which are penalized with a user-defined non negative scalar parameter ρ [20]. With the penalty included as mentioned above, the objective function can now be expressed as (3.8)

$$\phi = \min_{\Delta u, \epsilon_1, \epsilon_2} \sum_{i=0}^{H_u-1} \Delta u(k+i|k)^2 + \sum_{i=1}^{H_p} \rho\epsilon_1(k+i|k) + \sum_{i=1}^{H_p} \rho\epsilon_2(k+i|k) \tag{3.8}$$

Relaxing the voltage constraints modifies (3.7) to (3.9).

$$V^{min} - \epsilon_1(k+i|k) \leq V(k+i|k) \leq V^{max} + \epsilon_2(k+i|k) \tag{3.9}$$

To sum up, the final optimization problem can be formulated with the objective function (3.8) with the constraints (3.2), (3.5), (3.6) and (3.9). This MPC based optimization control can be expressed in standard form as a linear quadratic problem. It can be solved using various quadratic programming algorithms. In this study, interior point convex optimization algorithm is applied to find the optimal solution.

3.4 MPC controller settings

For the simulation study, a comparison has been made for different MPC based optimization strategies in section 4.1-4.5. In this comparison, all the system parameters, ie. remote buses, control buses, load profile and PV profile are kept the same. Adding to this, it is assumed that the active and reactive power from all the solar PVs and BESS are measured. Since the coordinated control is established in the controller, it is expected that DSO would like to have strict voltage limits. Typically in today's networks the limits lies in the range of [0.9, 1.05]. In this simulation, it is assumed that the voltage limits lies in the range of $[V_{min}, V_{max}] = [0.975, 1.025]$ p.u. to see how the MPC controller would perform for a stricter voltage range.The sensitivity gain was calculated using the static power flow method as mentioned in [11]. The sensitivity gain can vary with the change in loads present in the network. Hence, to have the accurate results, the sensitivity is calculated at each time step k. In the section 3.3, it is mentioned that limits have been set for the reactive power output as well as the change in reactive power output. The converter capacity for the PVs and BESS is set to 24 KVA. Also, the change in the reactive power cannot be more than 25% at subsequent time-steps. To make sure that the MPC based optimization controller does not react too quickly, it is configured to send control signals to PV and BESS every 10s. For all the simulations, the value of H_p is set to 6 while H_u is set to 2. This implies that the controller foresee the effects of changes in

the control variables 6 time-steps or in absolute value 60s ahead in future. The value of ρ in (3.8) is set to 10^5. The selected ρ in this case is large enough compared to the control devices weights of 10^3. This ρ value makes sure that the constraint violation (voltage relaxation) will happen only when an infeasible solution is obtained [20].

The control variables for the optimization model are chosen to be the reactive power set-point Q_b of BESS and Q_{pv} of solar PVs. At any time t, the change in the control variable can be expressed as a single column vector $\Delta\mathbf{u}$:

$$\Delta\mathbf{u} = [\Delta\mathrm{Q_b^T}, \Delta\mathrm{Q_{pv}^T}]^\mathrm{T} \tag{3.10}$$

The changes in the control variables can vary dynamically. The PV active powers can vary according to the solar power availability. At any time, limits for the reactive power can be calculated based on the active power available. For a PV, at time t $= k + 1$, the maximum $\mathrm{Q_{pv}^{max}}$ and minimum $\mathrm{Q_{pv}^{min}}$ reactive power can be calculated based on the available active power $\mathrm{P_{pv}^{g}}$ of PV at time t $= k$ and the rating of it's converter $\mathrm{S_{conv}}$ as shown in (3.11) and (3.12). A similar procedure can be followed to get the minimum and maximum limits for BESS reactive power.

$$Q_{pv}^{max} = +\sqrt{S_{conv}^2 - (P_{pv}^g(k))^2} \tag{3.11}$$

$$Q_{pv}^{min} = -\sqrt{S_{conv}^2 - (P_{pv}^g(k))^2} \tag{3.12}$$

3.5 System simulation

It is assumed that the local controllers at the PVs and BESS react much faster to changes in voltage than the MPC controller. For the system to not react too quickly, the MPC controller is configured to send the signals to the local controllers every 10s. This makes sure that there is sufficient time delay considered for the collection of measurement data and the calculation for the MPC controller; and the control signal communications between the MPC controller and the local controllers.

Following steps are considered to run the simulation in MATLAB. Few important steps to be carried out for the simulation are - to read the measurement data every 10s, perform power flow calculations, do gain calculations with the available loading conditions and update the set-point changes available from the MPC.

The simulation starts with t = 0s where the measurement data for the remote bus voltage, loading conditions and the measurement data of the active and reactive power output of PVs and BESS are read.
The above algorithm shows how the simulation is carried out for 220s duration. Here S_{PV} and S_{BESS} are the apparent powers at any time k which can give the P and Q components using the power factor of 0.85 lagging. S_{load} is the loading condition available at any time t. Z is the impedance data available for the network. This value will be fixed for the system at all times. The simulation is assumed to run for 220s at an interval of every 10s. At any time t, the Backward forward sweep powerflow is run for the given loading and the generation conditions. The measured bus voltages for the MPC controller is then taken from the powerflow output. MPC

Algorithm 1 : Algorithm for the simulation of the network

Data: V_{meas}, Z, S_{PV}, S_{BESS}, S_{load}
Initialisation: $\Delta u = 0$
for t = 0 to N **do**
  Update $Q_{control-buses}(t) = Q_{control-buses}(t) + \Delta$u(t-1)
  Run the backward forward sweep powerflow with S_{PV}, S_{BESS}.
  Input V_{meas} as the results from the powerflow.
  Run the MPC controller with input V_{meas}, S_{PV}, S_{BESS} and calculate the setpoint for $\Delta u(t)$.
end for
Update t
Repeat

controller takes in the input as the measured bus voltages, P and Q values measured for all the PVs and BESS which are controlled. The MPC controller then calculates the setpoint change in $\Delta u(t)$. The corresponding changes are then updated in the next time step *t+1*.

Simulations were done for the above mentioned modified CIGRÉ's European LV network. It was assumed that the active power profile was same for all the PVs in the network. Each solar PV has a rated capacity of 8KW. The PV data is measured every 0.2s. Since the MPC is operating every 10s, it is important to see how the sampled data at 10s will be seen by the MPC. The PV profile for one of the solar PVs is shown in Figure 3.3a, along with the measurement data seen by the MPC based controller. The effect of changing this time step is studied in section 4.7.1. The loads are treated as a constant power type, hence the power factor would be constant for all loads and is taken as 0.85 lagging for all loads. The load profile is shown in Figure 3.2b

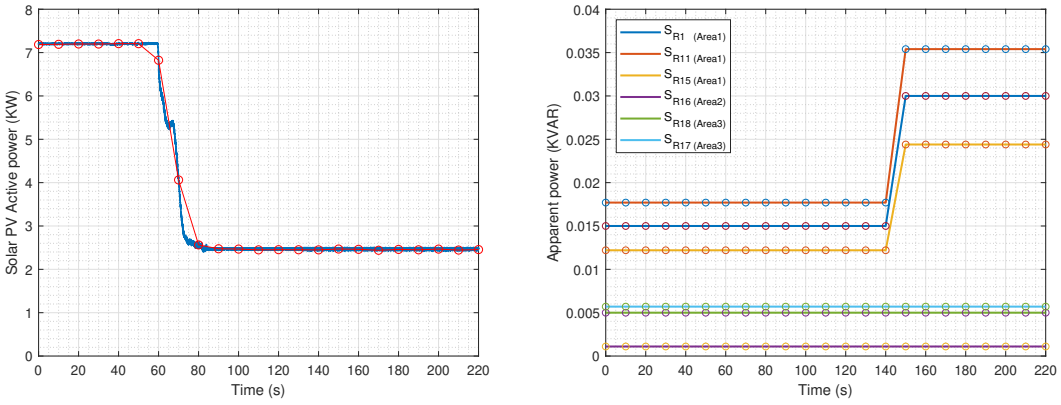

(a) PV profile **(b)** Load profile

Figure 3.3: The PV and load profile with the measurement points data

4

Results and discussion

To study different MPC algorithms mentioned in section 2.4.1 - 2.4.4, the test system in Figure 3.1 can be divided into 3 areas as shown in Figure 4.1. Table 4.1 shows the buses and the location of the PV and BESS in each area. Bus R_{E00a} is not considered in any area since it is a slack bus. It is assumed that the converters of the PV and BESS devices are available to all the optimizers for control of voltage.

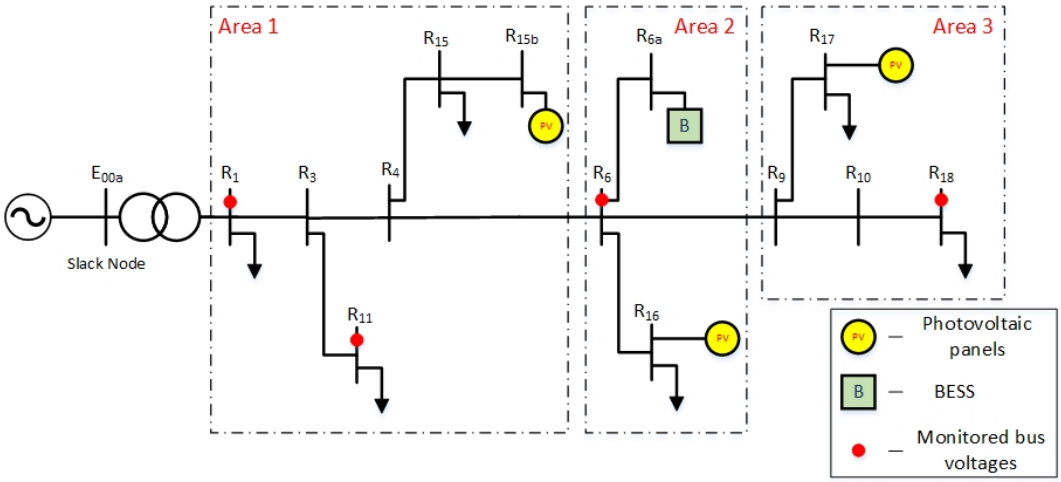

Figure 4.1: The modified CIGRÉ test system

AREA	Buses in the area	PV	BESS	Monitored
Area 1	R_1, R_3, R_4, R_{11}, R_{15} and R_{15b}	R_{15b}	-	R_1 and R_{11}
Area 2	R_6, R_{6a} and R_{16}	R_{16}	R_{6a}	R_6
Area 3	R_9, R_{10}, R_{17} and R_{18}	R_{17}	-	R_{18}

Table 4.1: Area wise division of buses

Voltage measurements are available to MPC for buses R_1 and R_{11} in area 1, R_6 in area 2 and R_{18} in area 3. Additionally, it is assumed that the reactive and active power output of the solar PV and BESS are measured.

The PV profile represents a scenario where there is a decrease in PV production after t = 60s due to the cloud coverage. The cloud coverage essentially implies that there would be voltage drop due to lesser PV penetration. Additionally, at t = 150s, all the loads in area 1 are increased by 2 times. This will further reduce

the voltages in the buses. The response for the scenario can be studied for PCVC, PDVC, S-PDiVC and P-PDiVC strategies for these conditions.

4.1 No control

This section describes the system when there is no MPC based control established. Figure 4.2 - 4.4 shows the voltages in different areas in the system. Voltages in all 3 areas remains inside the desired limits until t = 90s. From t = 0s to 60s, the voltage remains constant as the loads and the PV generation are fixed. As expected, when there is a cloud cover between time from t = 60s to t = 100s, the voltage drops due to lesser PV penetration. The drop will be higher in the area where there is more PV penetration. Since every area has one solar PV, the drops seen in buses near to PVs were close enough but the highest drop of 0.0102 p.u. is seen at bus R_{17}. Other bus voltage drops lie in the range of 0.0069 - 0.0092 p.u. and the minimum drop of 0.0055 p.u. is seen at bus R_1 since it is the farthest bus from all PVs. The bus R_{11} reaches the minimum voltage of the entire system at t = 100s and it's value is 0.9727 p.u.

At t = 150s, there is a large drop in the voltages due to increase in the load values in area 1. As expected the drops in area 1 is more, since it is the area where the change is observed. Area 1 bus voltages drops by around 0.026 p.u., while the area 2 and area 3 buses drops by 0.022 p.u. The minimum of all buses at t = 150s to t = 220s is at bus R_{11} and it's value is 0.9459 p.u.

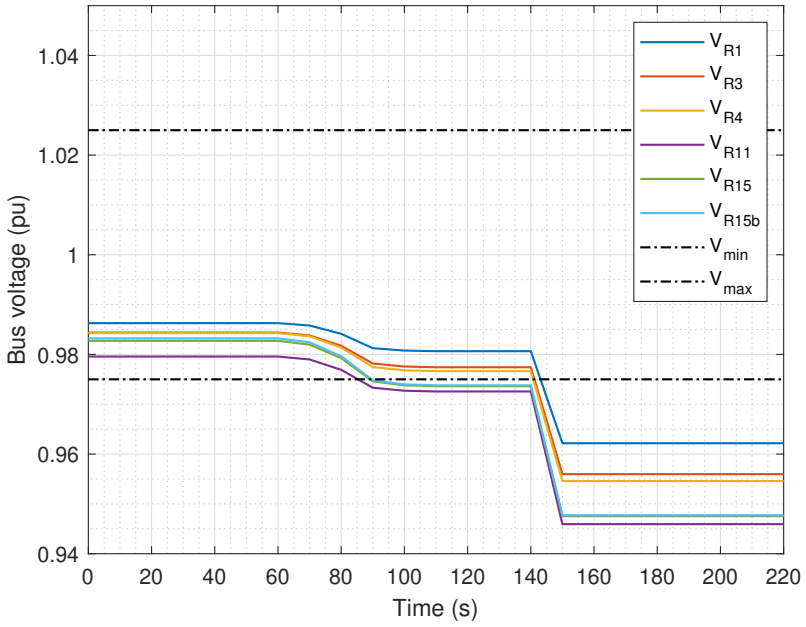

Figure 4.2: No control - Bus voltages in area 1

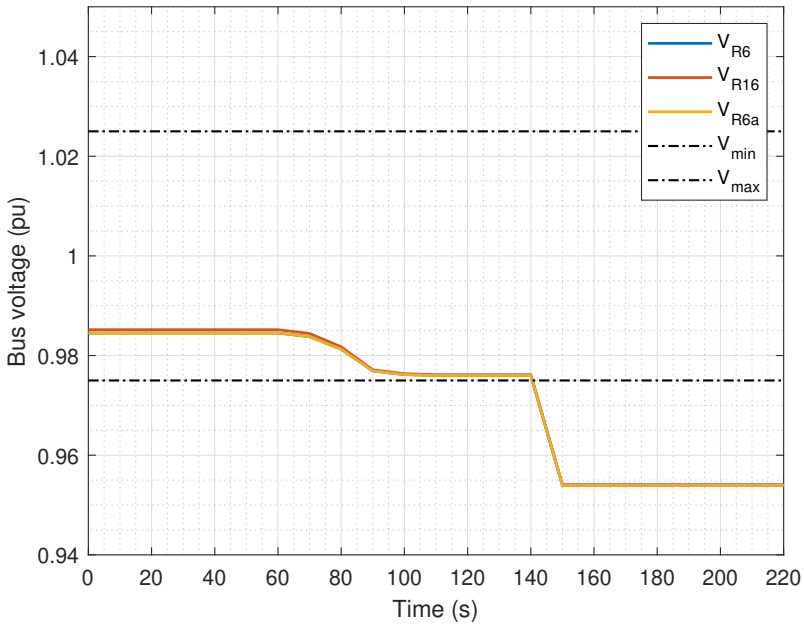

Figure 4.3: No control - Bus voltages in area 2

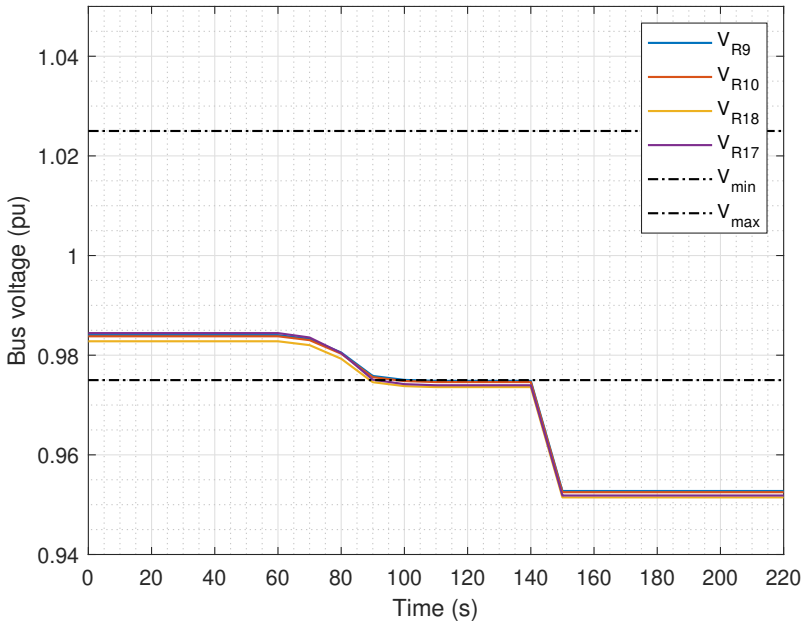

Figure 4.4: No control - Bus voltages in area 3

Since it is desired to have the voltage in the limits of [0.975, 1.025], some type of control needs to be implemented. In the following section, the proposed MPC based control methods have been implemented for the above system followed by the results and discussion.

4.2 PCVC strategy response

The PCVC strategy is explained in section 2.4.1. The objective function of PCVC considers the monitored buses in all areas and hence, the optimization result is expected to be better than decentralized and distributed MPC strategies. The results of PCVC strategy are discussed in this section. Figure 4.5-4.7 shows the bus voltages in each of the 3 areas. As seen in the previous section with no control, the voltage at all the buses starts inside the voltage limits, hence the MPC controller takes no action. At t = 60s due to cloud coverage, the voltages starts to drop and reaches it's minimum value at t = 100s. It can be seen that the bus voltage R_{11} in area 1 goes below the limits at t = 80s. Hence an MPC control action is necessary to get the voltage above the minimum limit of 0.975 p.u. Reactive power is provided equally by all the controllers as seen in Figure 4.9. By utilising this reactive power, the voltage is able to get into the voltage limits by t = 140s, as seen in Figure 4.8.

At t = 150s, the loads in area 1 increase leading to overall voltage decrease in the system. By utilising the reactive power available from the controllers, all the voltages were successfully brought inside the voltage range of [0.975 p.u., 1.025 p.u.]. The minimum bus voltage is 0.975 p.u. at bus R_{11}.

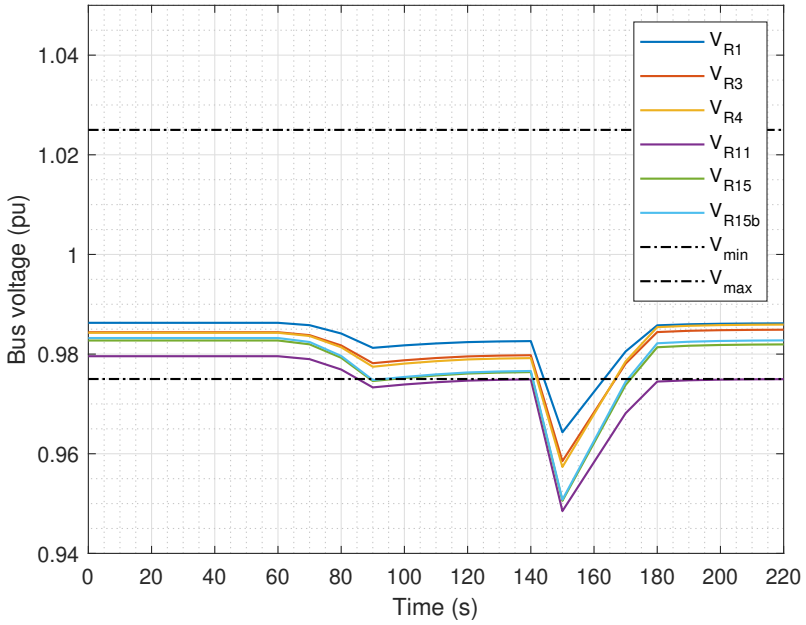

Figure 4.5: PCVC - Bus voltages in area 1

Figure 4.5 shows the voltages at all monitored buses in area 1. The lowest voltage can be seen at bus R_{11}. The goal to have the monitored buses inside limits has been achieved for area 1.

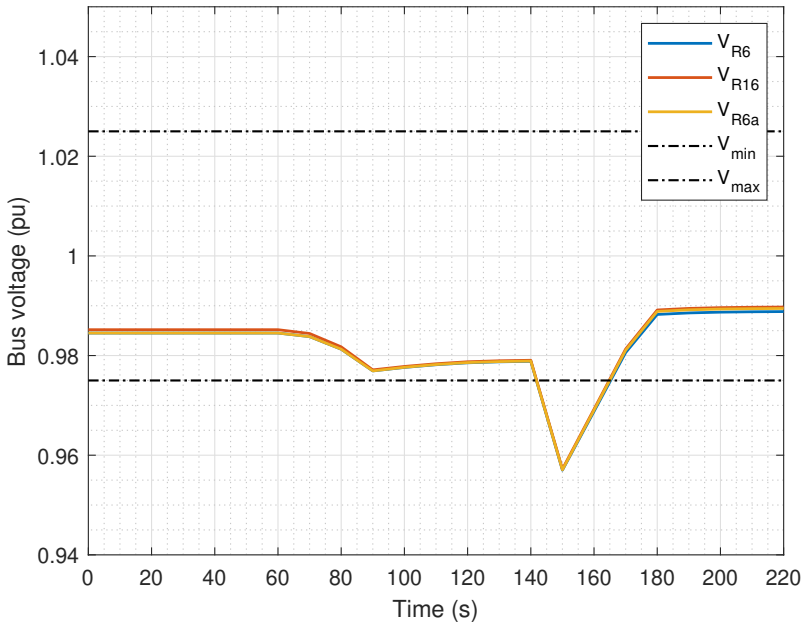

Figure 4.6: PCVC - Bus voltages in area 2

Figure 4.6 shows the voltages at all monitored buses in area 2. All three bus voltages have reached inside the desired range.

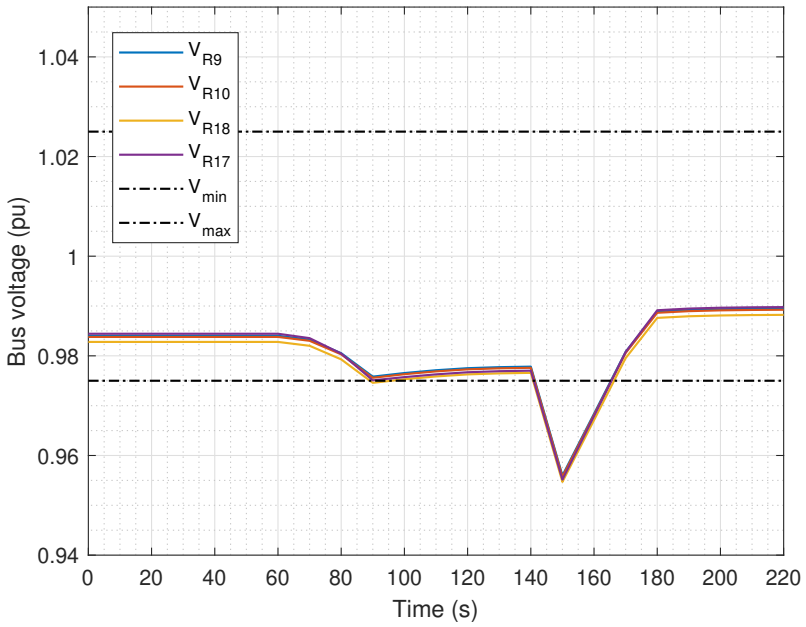

Figure 4.7: PCVC - Bus voltages in area 3

Figure 4.6 shows the voltages at all monitored buses in area 3. In this area too, all monitored bus voltages can be seen to have reached inside the limits.

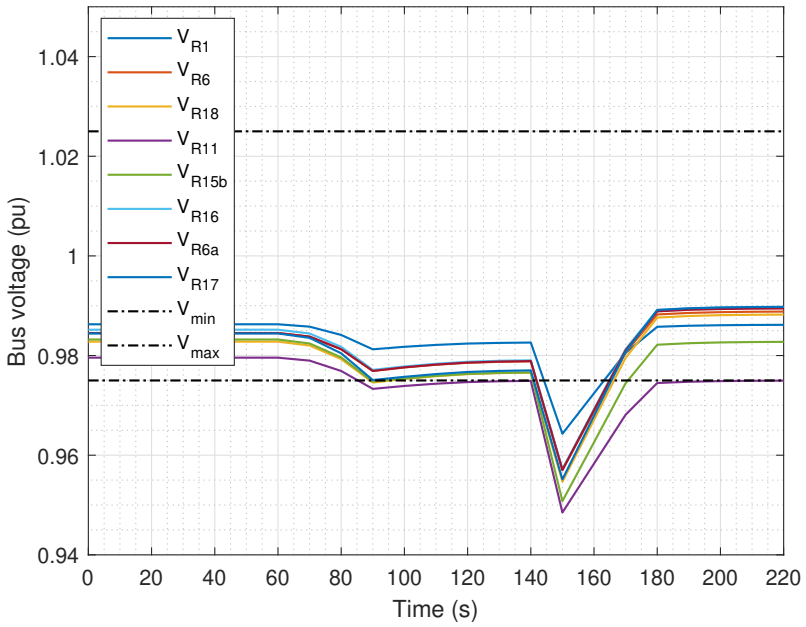

Figure 4.8: PCVC - Monitored bus voltages

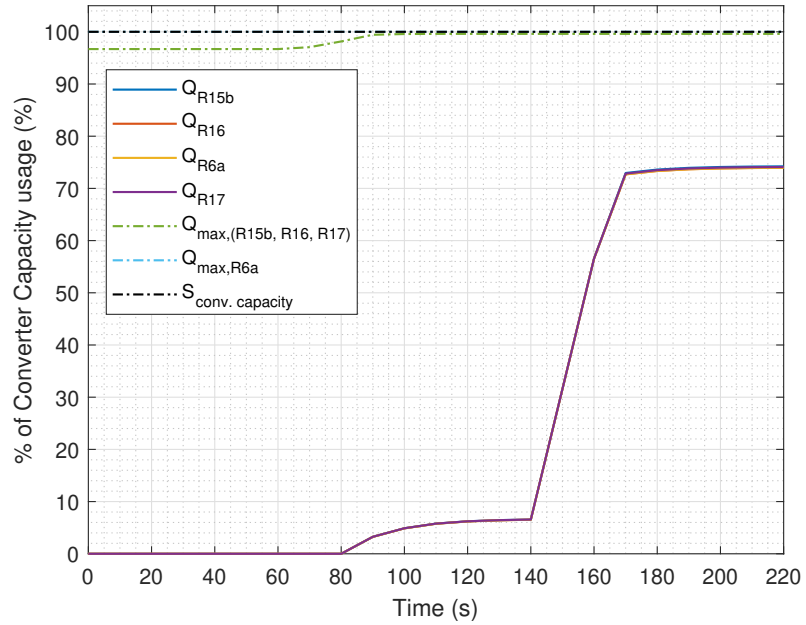

Figure 4.9: PCVC - Reactive power used in all control buses

Figure 4.8 shows all the measured buses in the network. It can be seen that the PCVC strategy is able to get all the buses inside the voltage limits optimally. Figure 4.9 shows how much reactive power is utilized in terms of the % of total converter capacity (24KVA for each converter = 100%). The reactive power usage at all 4 buses, R_{6a}, R_{15b}, R_{16} and R_{R17} utilizes the same amount of reactive power and

hence are overlapping in the figure. It is to be noted that all the controller have been assigned equal weights of 1000. Also, it can be noted in Figure 4.9 that the maximum reactive power value Q_{max} for all the three PV changes with time. This is due to the dynamic nature of the reactive power limits as expressed in (3.11) and (3.12). The total available capacity of all the controllers is 96 KVA. A total of 71.1 KVAR was utilised from the controllers to get all the bus voltages into the limits translating to a 74 % of the total capacity available.

4.3 PDVC strategy response

As explained in section 2.4.2, the PDVC strategy has as many optimizer as there are areas in the network. Each area has one PDVC which can regulate the monitored bus voltages in that area with using the control devices present in that area alone. There is no communication between different areas hence the reactive power of one area cannot be utilised by the other area. The results for the PDVC strategy has been discussed below. Figure 4.10 shows the voltages for the buses in area 1. The voltage in bus R_{11} goes below the voltage limit at t = 100s due to the cloud coverage but is brought back inside the allowed voltage range by t = 140s. At t = 150s there is a drop in voltage due to increase in the loads in area 1 as shown in Figure 3.2b. The bus voltage at R_{11} doesn't reach inside the voltage limits due to insufficient resources. From Figure 4.14, it can be noted that all the resources in area 1, i.e. reactive power from the controller at bus R_{15b} is utilised but still, the optimization model is unable to get the bus R_{11} into limits.

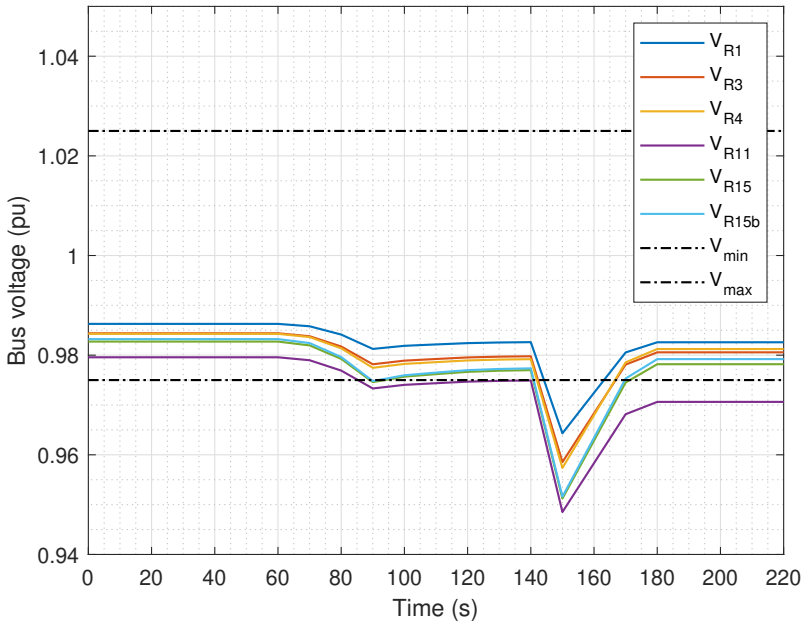

Figure 4.10: PDVC - Bus voltages in area 1

In figure 4.11, all bus voltages in area 2 reaches the limits but the voltages rise slightly lower than what was seen in PCVC strategy for area 2 as seen in Figure

4.6. This is because of no communication between the optimizers of 3 areas. Due to this lack of communication, the reactive power of area 2 and 3 cannot be shared with area 1.

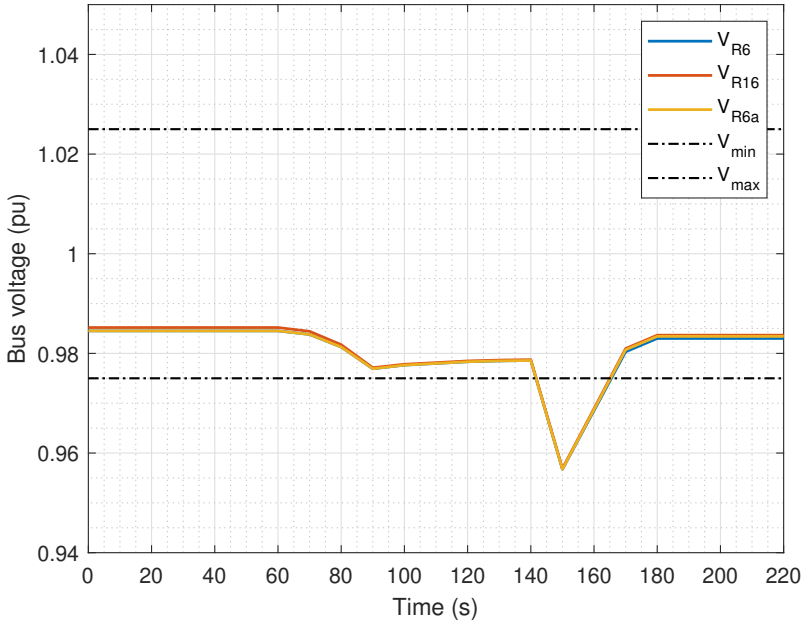

Figure 4.11: PDVC - Bus voltages in area 2

In figure 4.12, all bus voltages in area 3 reaches the limits but the voltages rise slightly lower than what was seen in PCVC strategy for area 3 (Figure 4.7).

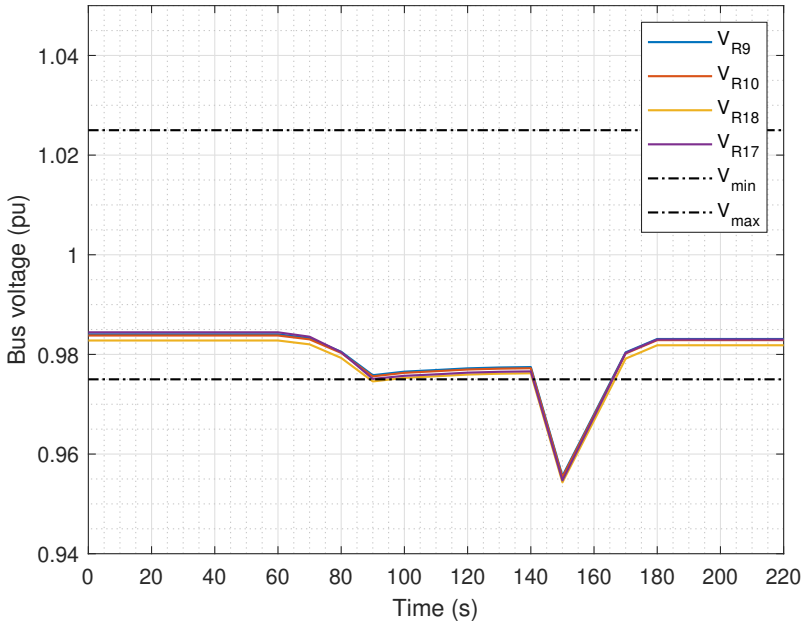

Figure 4.12: PDVC - Bus voltages in area 3

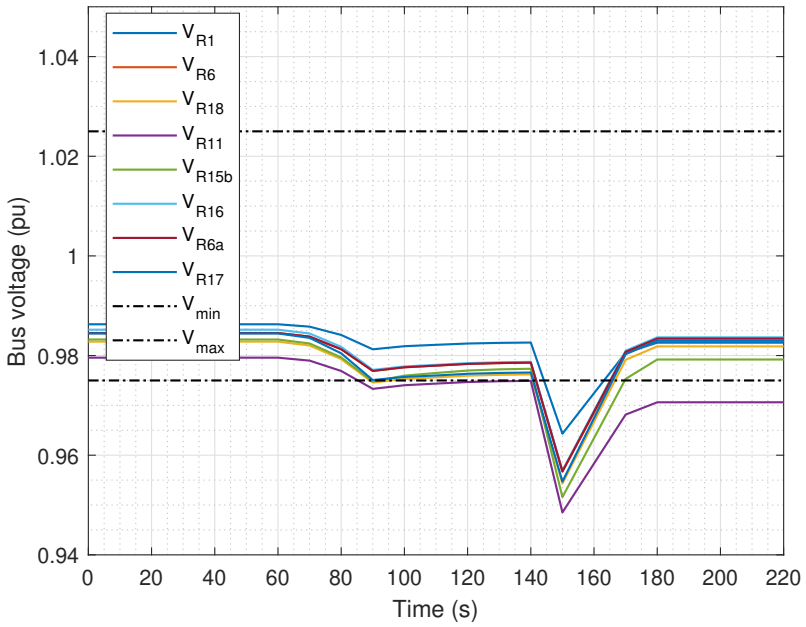

Figure 4.13: PDVC - Monitored bus voltages

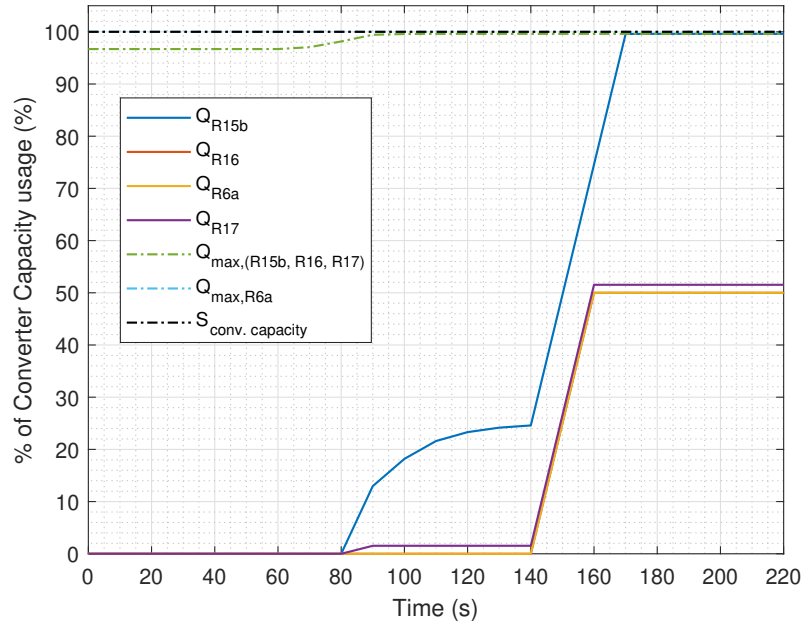

Figure 4.14: PDVC - Reactive power used in all control buses

Figure 4.13 shows the voltages at all the monitored buses in the system. Comparing Figure 4.13 with the voltages in PCVC strategy (Figure 4.8), it can be seen that all voltages has slightly lower value. This decrease was led by lower reactive power injection. The lower injection is because of the absence of the communication between different areas in the network. Hence the optimal output cannot be reached.

Figure 4.14 shows the reactive power injected by different converters. The converter at bus R_{15b} injects the highest amount of reactive power because of it's higher sensitivity gain value as mentioned in the previous section. In PCVC strategy it was observed that the reactive power injection at other three buses was equal but this is not the case in PDVC. This is because of the lack of communication between the areas in PDVC strategy. A total of 60.3 KVAR was injected from the controllers to get the bus voltages into the limits translating to a 62.8 % of the total capacity available.

4.4 S-PDiVC strategy response

As explained in section 2.4.3, the S-PDiVC strategy has as many optimizer as there are areas in the network. Each area has one S-PDiVC which can regulate the monitored bus voltages in that area with using the control devices present in that area. There is limited communication between different areas hence the reactive power of one area can be utilised by the other area but not as efficiently as in PCVC. The results for the S-PDiVC strategy has been discussed below.

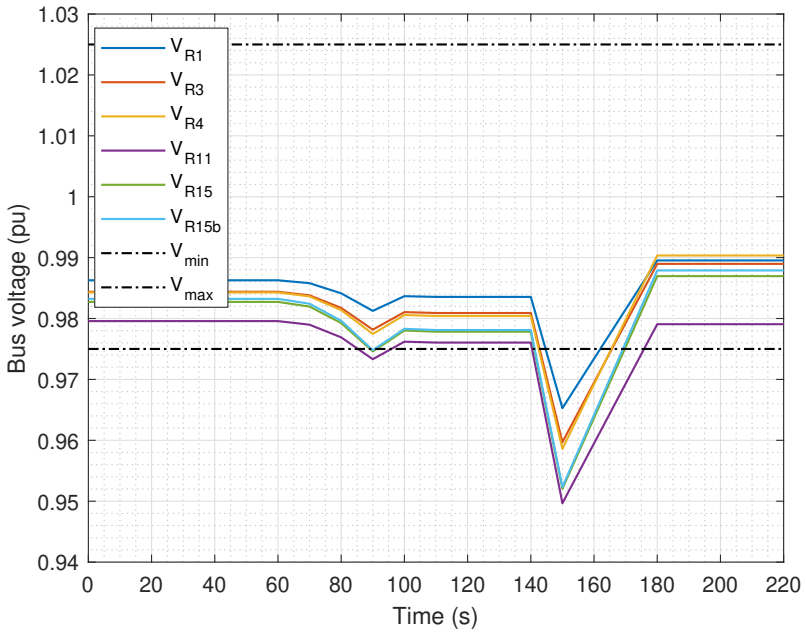

Figure 4.15: S-PDiVC - Bus voltages in area 1

Figure 4.15 shows the voltages for the buses in area 1. The voltage in bus R_{11} goes below the accepted voltage limit at t = 100s due to the cloud coverage but is brought back inside the allowed voltage range by t = 140s. At t = 150s there is a drop in voltage due to increase in the loads in area 1 as shown in Figure 3.2b. All bus voltages reach inside the voltage limits. It can be noted that the voltage settles slightly higher than the minimum limit of 0.975 p.u. This overshoot happens due to overcompensation of the reactive power in the MPC algorithm. All bus voltages are higher compared to the bus voltages in PCVC strategy.

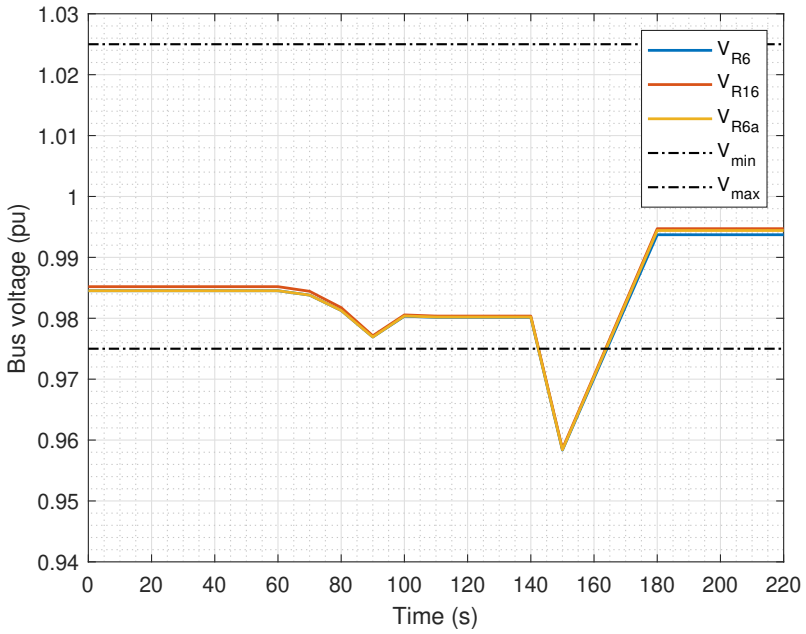

Figure 4.16: S-PDiVC - Bus voltages in area 2

Figure 4.16 shows the voltages for the buses in area 2. All bus voltages are higher compared to the bus voltages in PCVC strategy.

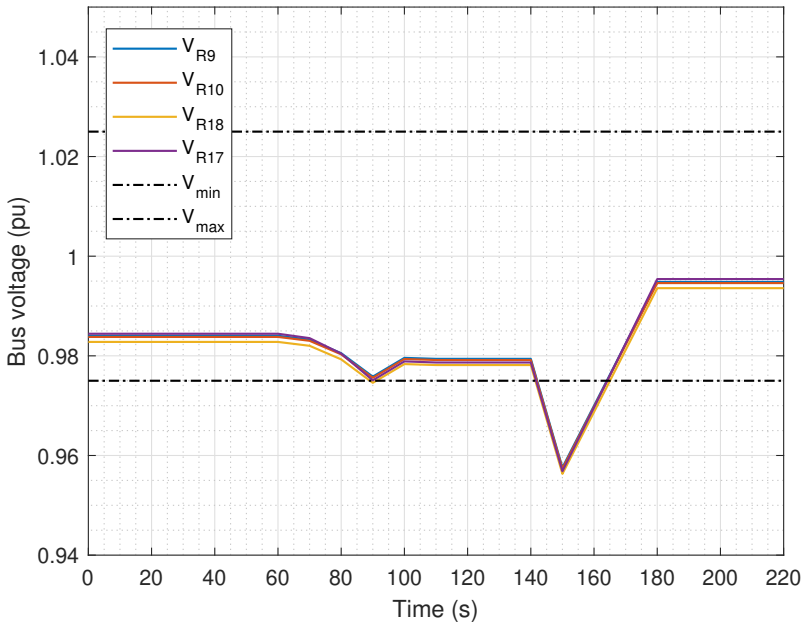

Figure 4.17: S-PDiVC - Bus voltages in area 3

Figure 4.17 shows the voltages for the buses in area 3. All bus voltages are higher compared to the bus voltages in PCVC strategy.

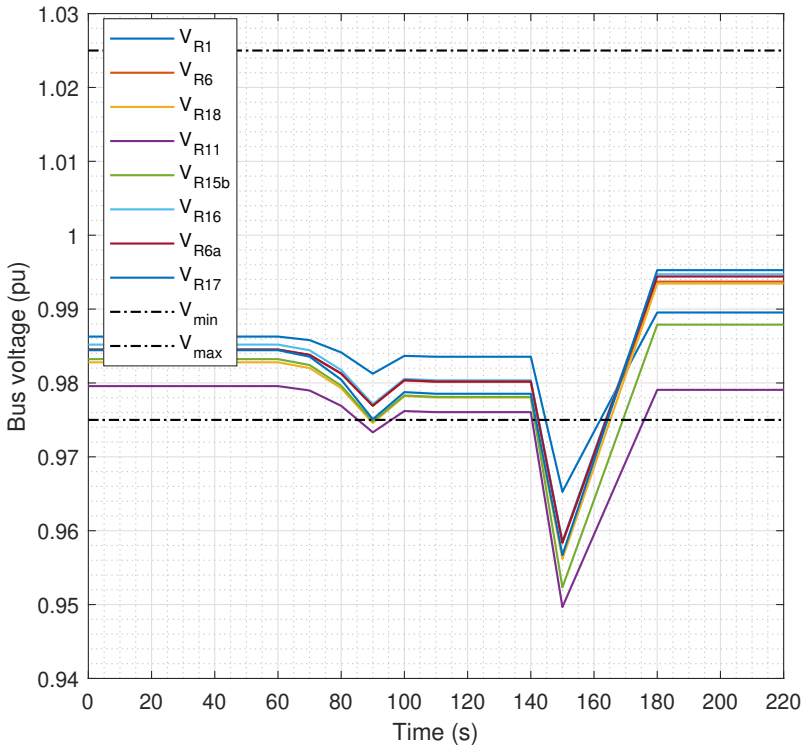

Figure 4.18: S-PDiVC - Monitored bus voltages

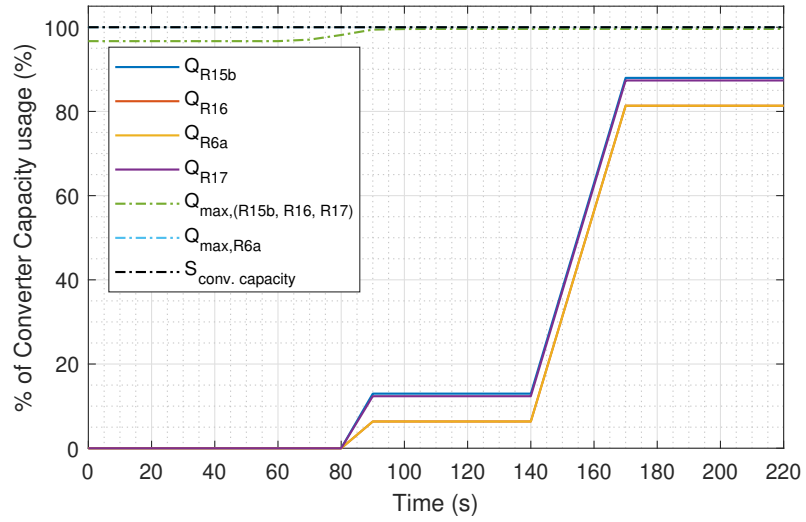

Figure 4.19: S-PDiVC - Reactive power used in all control buses

Figure 4.18 shows the voltages for the monitored buses in all areas. It can be noted that the voltage settles slightly higher than the minimum limit of 0.975 p.u. This overshoot happens due to overcompensation of the reactive power in the MPC algorithm. All bus voltages are higher compared to the bus voltages in PCVC strategy.

Figure 4.19 shows the reactive power injected by different converters. The converter at bus R_{15b} injects the highest amount of reactive power since area 1 need more reinforcement than the other areas due to increase of the load. In PCVC strategy it was observed that the reactive power injection at other three buses was equal but this is not the case in S-PDiVC. This is because of the limited communication between the areas in S-PDiVC strategy. A total of 81.3 KVAR was utilised from the controllers to get all the bus voltages into the limits translating to a 84.7 % of the total capacity available.

4.5 P-PDiVC strategy response

Although PCVC provides the optimal output, it's practical implementation is very complex. Also, due to a single optimizer, it's reliability is low. On the other hand PDVC has a simple architecture. Hence to have the architectural advantage of PDVC and considering the communication between different areas, a compromise is made in form of P-PDiVC strategy. The P-PDiVC strategy is explained in Section 2.4.4.

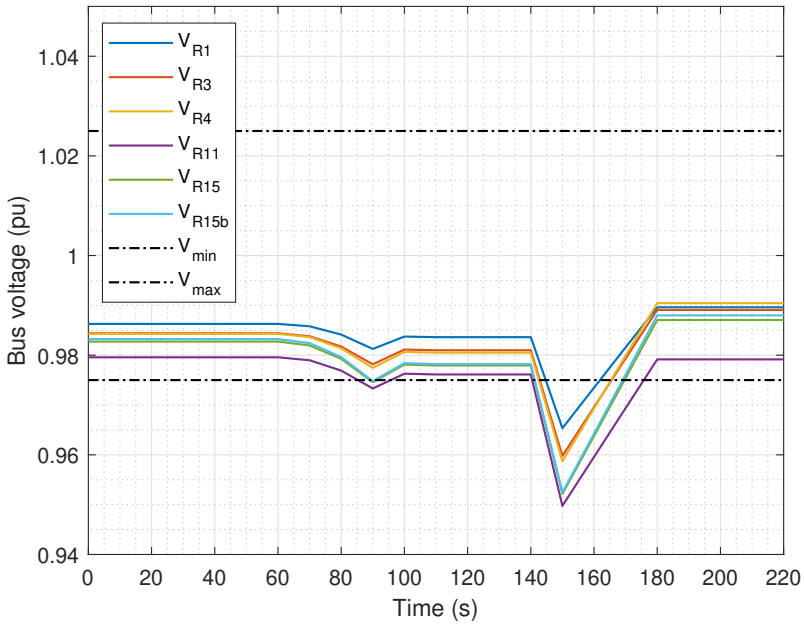

Figure 4.20: P-PDiVC - Bus voltages in area 1

Figure 4.20 shows the voltages for the buses in area 1. The voltage in bus R_{11} goes below the accepted voltage limit at t = 100s due to the cloud coverage but is brought back inside the allowed voltage range by t = 140s. At t = 150s there is a drop in voltage due to increase in the loads in area 1 as shown in Figure 3.2b. All bus voltages reach inside the voltage limits. It can be noted that the voltage settles slightly higher than the minimum limit of 0.975 p.u. This overshoot happens due to overcompensation of the reactive power in the MPC algorithm. All bus voltages are higher compared to the bus voltages in PCVC strategy. Figure 4.21 and 4.22

show the voltages for the buses in area 2 and area 3 respectively. All bus voltages are higher compared to the bus voltages in PCVC strategy.

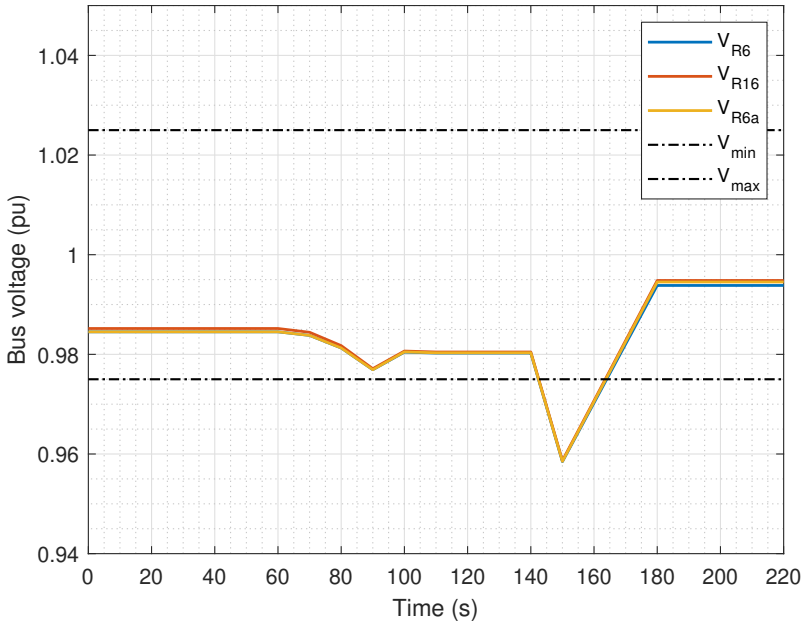

Figure 4.21: P-PDiVC - Bus voltages in area 2

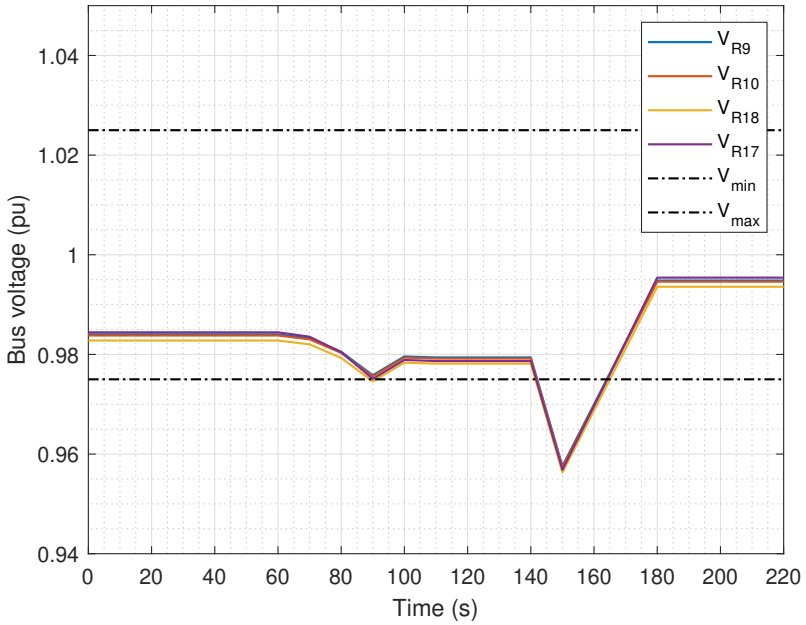

Figure 4.22: P-PDiVC - Bus voltages in area 1

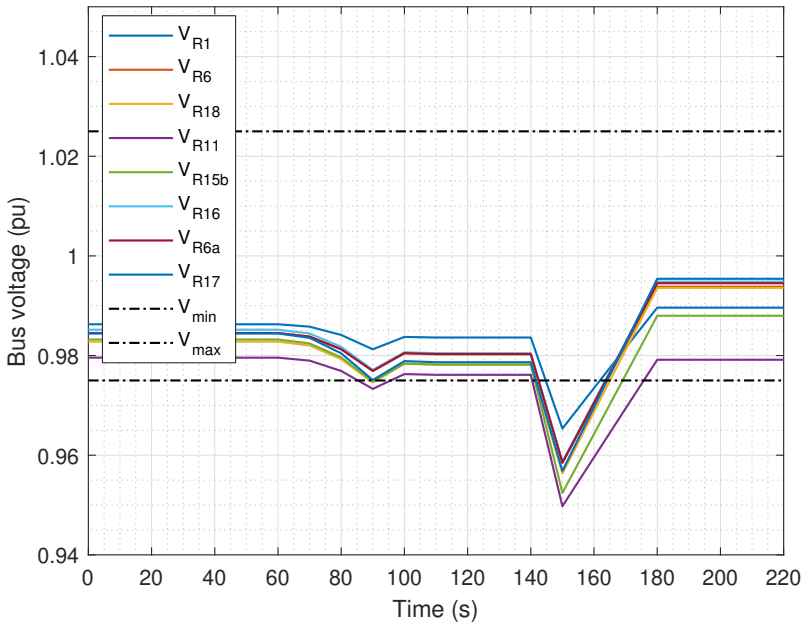

Figure 4.23: P-PDiVC - Monitored bus voltages

Figure 4.23 shows the voltages for the monitored buses in all areas. It can be noted that the voltage settles slightly higher than the minimum limit of 0.975 p.u. This overshoot happens due to sub-optimal overcompensation of the reactive power. All bus voltages are higher compared to the bus voltages in PCVC strategy.

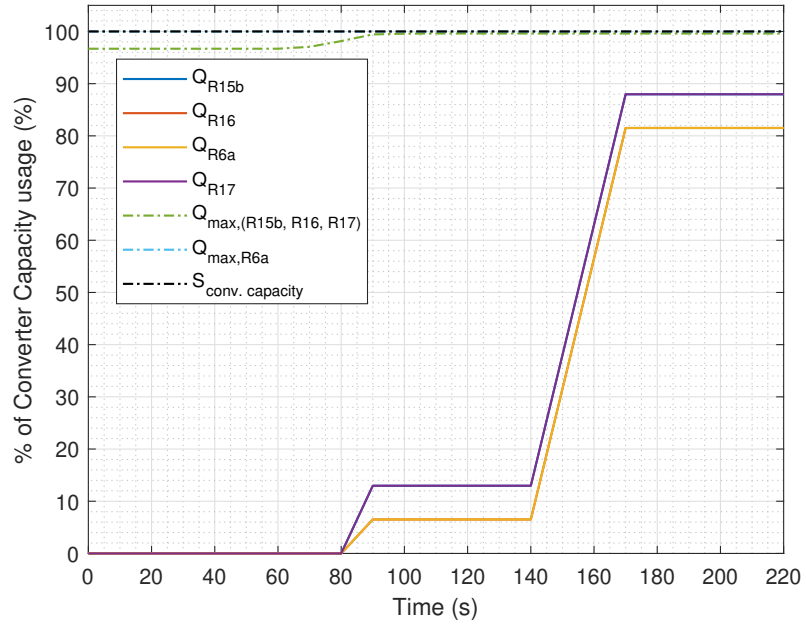

Figure 4.24: P-PDiVC - Reactive power used in all control buses

Figure 4.19 shows the reactive power injected by different converters. In PCVC

strategy it was observed that the reactive power injection at other 4 buses was equal but this is not the case in P-PDiVC. This is because of the limited communication between the areas in P-PDiVC strategy. A total of 81.1 KVAR was utilised from the controllers to get all the bus voltages into the limits translating to a 84.4 % of the total capacity available.

4.6 Comparison of results of the MPC strategies

The four MPC strategies have been compared on the basis of how much reactive power is consumed from the available controllers and the average simulation time it takes for the processing of the MPC strategies. Q_{all} in table 4.2 is the reactive power utilization by all the 4 available controllers combined. It is mentioned as the percent utilization compared to the total available capacity, ie. 96 KVAR. Q_{usage} is the reactive power utilization compared to PCVC strategy as base. Since PCVC utilizes 74.1 KVAR, it is considered as 1 p.u. (only for current comparison)

MPC Strategy	$\mathbf{Q_{all}}$(%)	$\mathbf{Q_{usage}}$**(w.r.t. PCVC)**	**Simulation time (s)**
PDVC	62.8	0.838	0.16
PCVC	74.1	1.000	0.13
S-PDiVC	84.7	1.143	0.33
P-PDiVC	84.4	1.135	0.36

Table 4.2: Comparison of different MPC strategies

The following can be concluded from the above results:

- It can be seen that, PDVC utilizes around 16.2 % less reactive power compared to PCVC, to bring the voltages of the monitored buses as well as the buses with PV and BESS connected to them inside the voltage limits. In PDVC, the voltage for bus R_{11} remains outside the voltage limits due to the lack of reactive power reserves in area 1. PCVC is able to bring all the voltages inside the limits by utilising the reserves in area 2 and area 3 as well. S-PDiVC and P-PDiVC displays similar results compared to PCVC but utilise around 14.3 % and 13.5 % more reactive power than PCVC, respectively. This is due to sub-optimal overcompensation in both cases resulting on a slightly higher voltage values compared to PCVC.

- Comparing the average processing times, PCVC and PDVC takes almost the same time to complete the computations. In P-PDiVC, there happens an exchange of information between the optimizers leading to higher computation times compared to PCVC and PDVC. P-PDiVC is 30ms slower than S-PDiVC since at every time-step, information needs to be shared among the optimizers. Here it should be considered that the system is comparatively small in size. With bigger systems, having more number of buses and control variables, the computation times will greatly increase.

4.7 Effect of various parameter on the MPC-based control

Four different MPC such as PCVC, PDVC, P-PDiVC and S-PDiVC, based control strategies were discussed above. In the system all the parameters like number of control buses, converter capacities, time duration between each MPC measurements, etc. were kept the same. In this section, few important parameters will be changed one at a time and it's effect on the system will be studied. To study different scenarios, network shown in Figure 4.1 is considered. PCVC strategy is implemented for all the scenarios. In Scenario 1, the time-step that the MPC operates at, has been varied to see how the system is affected. In scenario 2, the number of measured buses are varied and in scenario 3, the weights to the control buses is changed.

4.7.1 Scenario 1: Effect of time-step of the measurement data

Selecting the time-step is an important step of designing the controller. This time-step decides when the MPC controller will read the measurement data for the monitored bus voltages and the P and Q of PV and BESS. In this scenario, the effect of time-step at which the MPC runs is studied. In above Sections 4.1-4.5, a 10s time-step duration was considered. This means that the MPC controller reads the measurement data every 10s and then runs the algorithm to give the control set points for the next time-step. To see how the controller reacts to different time-steps, 3 cases are considered. Following cases are considered for this scenario:

1. Small time-step where the data is read very frequently at 5s
2. Normal time-step of 10s
3. Slow data measurement reading with a time-step of 20s

4.7.1.1 Case 1: 5s time-step

In this case, a comparatively small time-step of 5s is taken. This means that the MPC will be reading data every 5s and take actions according to the available values.

Figure 4.25 shows that the measurement of the PV and load data is taken every 5s and Figure 4.26 shows voltage response towards it for all measured buses. This means that the MPC will act every 5s, and for every 5s the maximum injection of the reactive power is 25% (maximum allowable reactive power injection between two consecutive MPC actions taken) is possible. This means that the objective to have the voltages in the limits can be reached faster. It can be noted that after the voltage drops to it's lowest value at t = 150s, voltage is brought back into the limits at t = 165s. It took 15s for the controller to get the voltage into the limits.

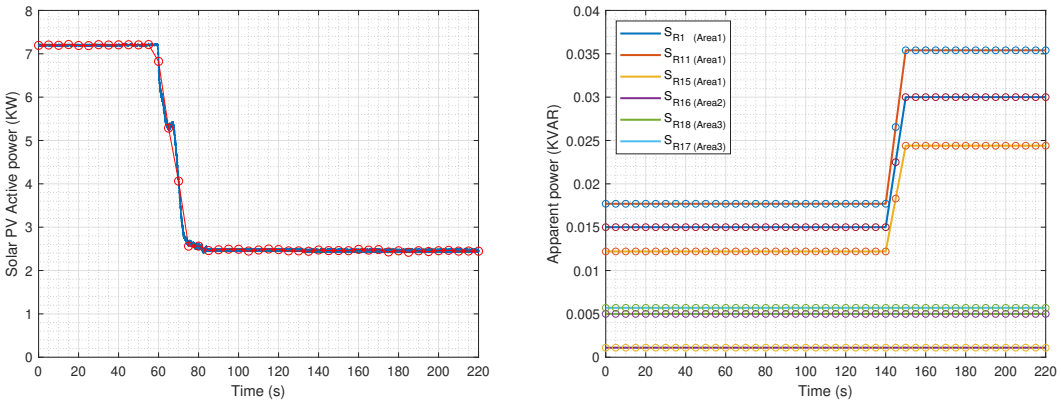

(a) PV profile **(b)** Load profile

Figure 4.25: The PV and load profile with the measurement points data

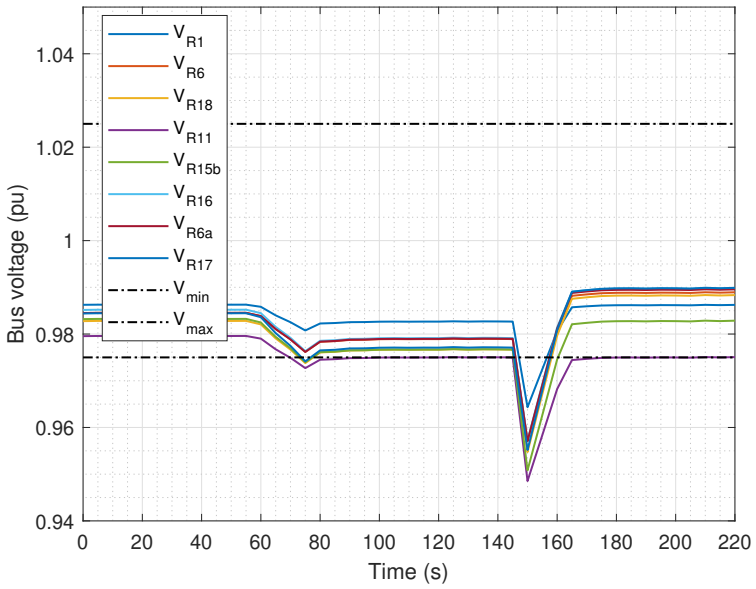

Figure 4.26: The MPC response

4.7.1.2 Case 2: 10s time-step

In this case, a time-step of 10s is considered. The detailed results have already been discussed in the previous sections. The MPC will be reading data every 10s and take actions according to the available values. Figure 4.27 shows that the measurement of the PV and load data is taken every 10s and Figure 4.28 shows the MPC response towards it. This means that the MPC will act every 10s and for every 10s, the maximum injection of the reactive power is 25% is possible. This means that the objective to have the voltages in the limits can be reached comparatively slower than case 1.

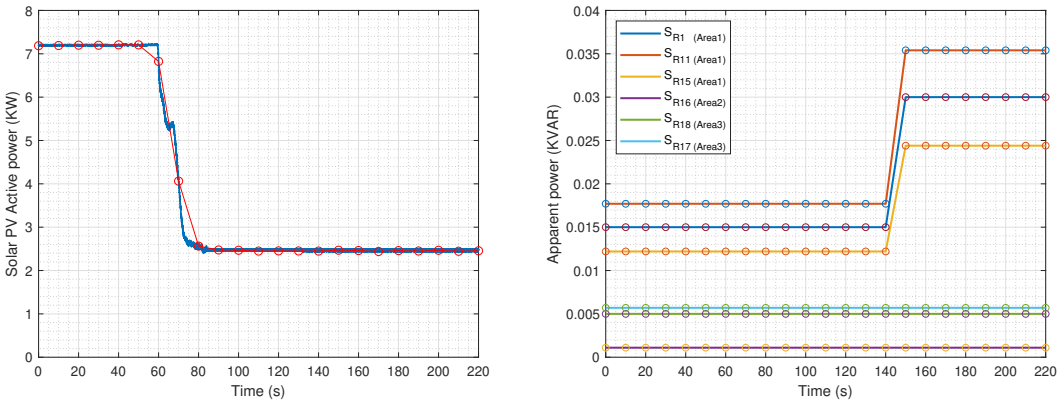

(a) PV profile **(b)** Load profile

Figure 4.27: The PV and load profile with the measurement points data

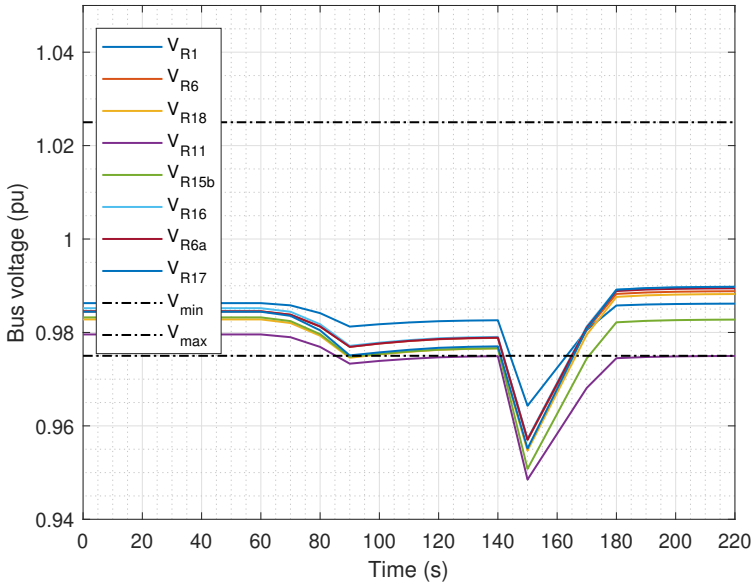

Figure 4.28: The MPC response

It can be noted that after the voltage drops to it's lowest value at t = 150s, voltage is brought back into the limits at t = 180s. It took 30s for the controller to get the voltage into the limits which is slower than in case 1.

4.7.1.3 Case 3: 20s time-step

In this case, a time-step of 20s is considered. The detailed results have already been discussed in the previous sections. The MPC will be reading data every 20s and take actions according to the available values.

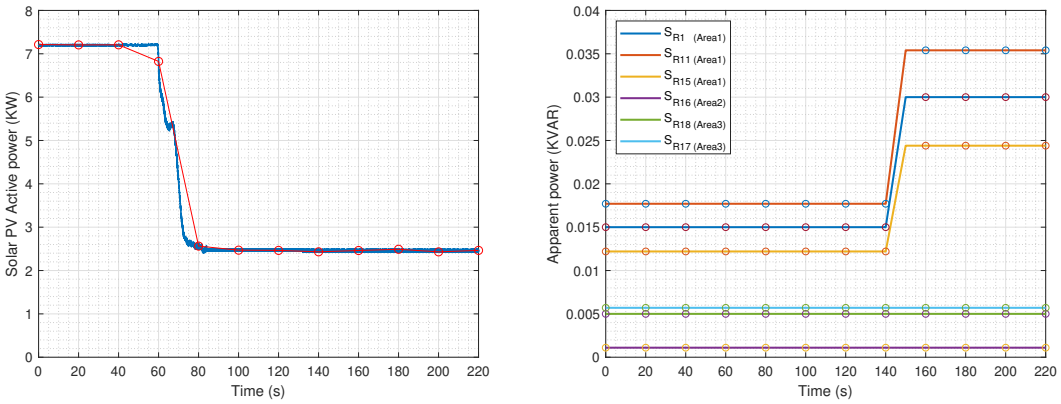

(a) PV profile **(b)** Load profile

Figure 4.29: The PV and load profile with the measurement points data

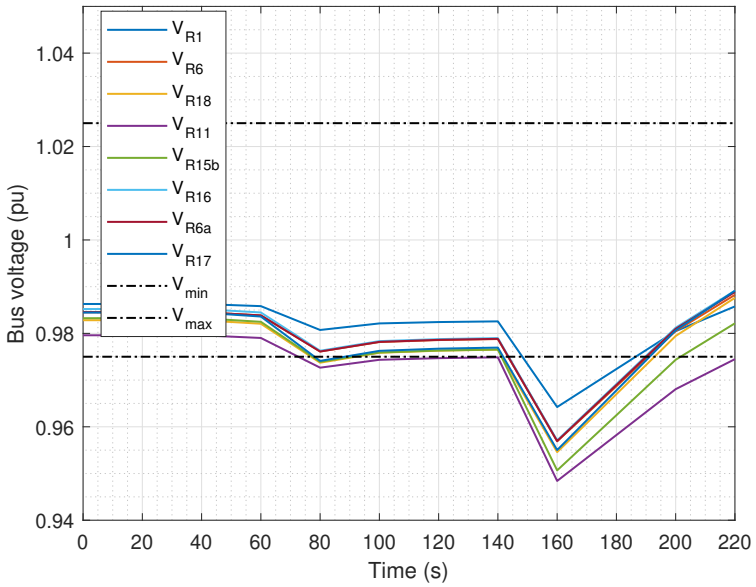

Figure 4.30: The MPC response

Figure 4.29 shows that the measurement of the PV and load data is taken every 20s and Figure 4.30 shows the MPC response towards it. This means that the MPC will act every 20s. Also, for every 20s, the maximum injection of the reactive power is 25% of the converter rated capacity. This means that the objective to have the voltages in the limits can be reached comparatively slower than case 1 and case 2.

It can be noted that after the voltage drops to it's lowest value at t = 150s, voltage is brought back into the limits at t = 240s. It took 60s for the controller to get the voltage into the limits which is slower than in case 1 and case 2.

4.7.1.4 Scenario 1: Discussion

As it can be seen from above figures that time-step has a huge impact on how fast the voltage can reach the voltage bounds. After a drastic drop of voltage due to increase in the loads in area 1 at t = 150s, it took case 1, case 2 and case 3; 15s, 30s and 60s to get to voltage limits, respectively. This result was as expected because of the limits established on how much reactive power can be injected between two consecutive time instant. A maximum of 25% change was set as the limits for all the PV and BESS controllers. Clearly the 5s time-step was the fastest followed by 10s time-step and 20s time-step, but it should be noted that distributed strategies like S-PDiVC and P-PDiVC requires sharing of information between different area optimizers. Hence, with smaller time-steps the computational power utilised would be higher.

In case of a sudden change in system or a short circuit, if the time-step is larger it might fail to see the incident and may result into system failure. For example, in case 3, when there is a sudden drop in PV input from t = 60s and it fails to notice this quick drop. This can cause a huge instability in the system.

Compared to case 2, case 1 has higher resolution, i.e. reading data frequently, leading to a faster control but higher computational speed requirement. Comparing the case 2 and case 3, there is a chance of missing out sudden event leading to huge voltage drops in case 3 leading to system instability and slower action towards getting bus voltages into limits.

Based on the above discussion and keeping in mind the system constraints and requirements, 10s time-step seems to be a better fit.

4.7.2 Scenario 2: Selection of measured buses

It is important to see how the controller acts based on which measured buses are selected and the number of measured buses in the network. In this scenario, network model and MPC parameters selected are same as mentioned in Chapter 3. Only the number of monitored buses are altered. PCVC based MPC strategy is selected since it provides optimal results and hence it would be easier to compare results. To see how the PCVC controller reacts to different number of monitored buses, 3 cases are considered. Following cases are considered for this scenario:

1. Only 1 measured buses
2. 4 measured buses
3. 9 buses - All buses in the network

4.7.2.1 Case 1: Only 1 measured bus

In this case, only 1 measured bus is considered. Two subcases are created to see whether selecting a particular bus affects the control. In section 4.1 where no MPC control was considered, it was seen that the bus R_{11} reaches the lowest bus voltage in the network when the loads are increased in area 1 at = 150s. In first subcase, the monitored bus is R_{11} and in second subcase, the monitored bus is R_6 in area 2.

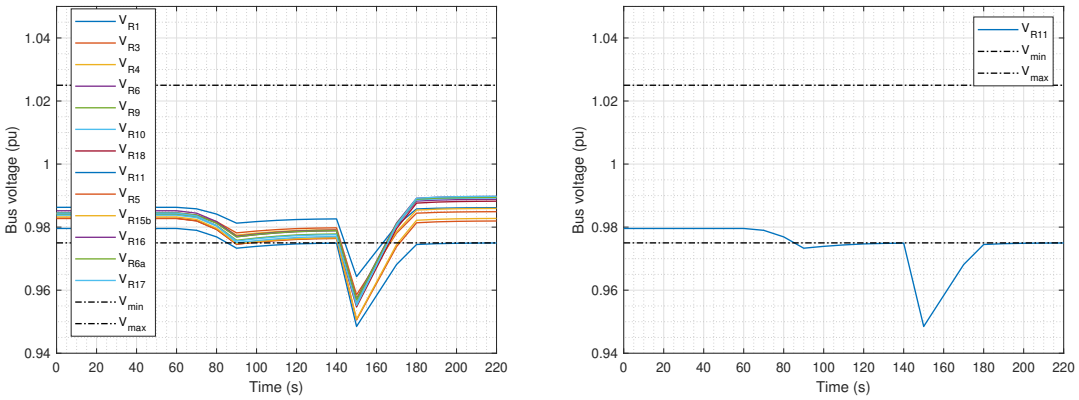

(a) All network buses **(b)** Monitored buses

Figure 4.31: Case 1.1: Measured bus: R_{11}

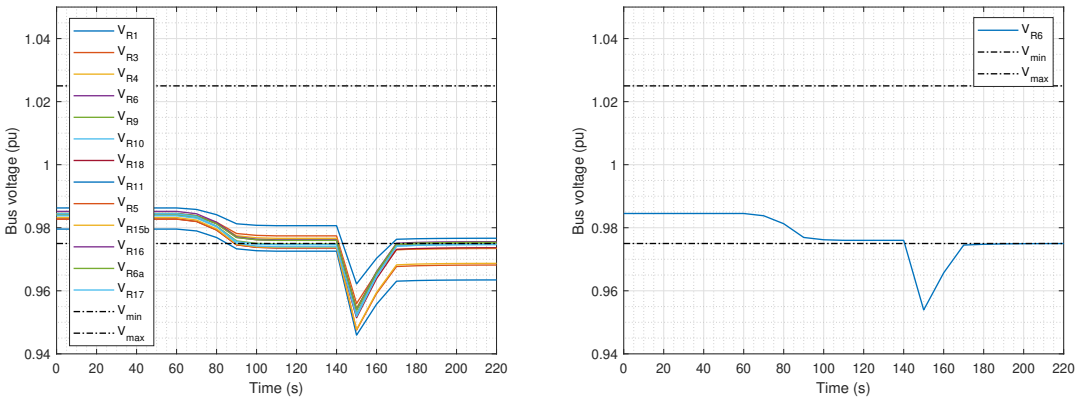

(a) All network buses **(b)** Monitored buses

Figure 4.32: Case 1.2: Measured bus: R_6

Figure 4.31 refers to case 1.1 where the monitored bus is R_{11} and Figure 4.32 refers to case 1.2 where the monitored bus is R_6. It can be seen that in both cases the PCVC strategy is successful in reaching the goal of having the monitored bus voltages inside the voltage limits, but in case 1.2, most buses are still quite lower compared to case 1.1. In case 1.1, where the monitored bus is R_{11} and has the lowest voltage value of all the buses in the network is able to reach the limits, leading to all other buses with higher voltage value than in case 1.2. Case 1.1 utilises a total of 71.2 KVAR reactive power from the PV and BESS controllers and case 1.2 utilises 42.8 KVAR. More usage of reactive power in case 1.1 leads to higher voltage rise in all buses.

Hence, with higher reactive power injection it is possible to have all the bus voltages in the system inside the limits. This clearly implies that selecting the monitored bus make a significant impact on the system voltages. The simulation times for both the cases were close to each other as it depends on how many number of monitored buses are there in the network and not on which bus is selected. Case 1.1 takes 17ms to compute the PCVC algorithm while case 1.2 takes 14ms to do the same.

4.7.2.2 Case 2: 4 measured buses

In this case 4 measured buses are considered namely R_1, R_6, R_{11} and R_{18}. Figure 4.33 shows the voltages in all the buses and the monitored buses.

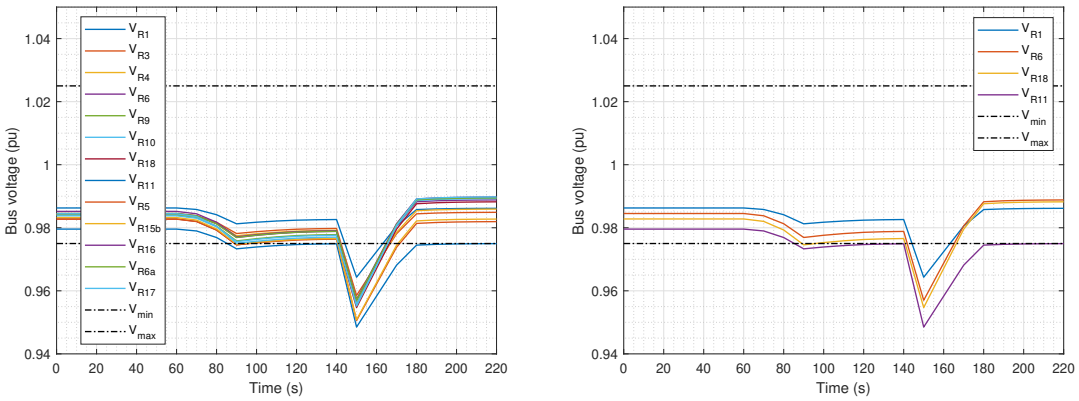

(a) All network buses **(b)** Monitored buses

Figure 4.33: Case 2: Measured bus: R_1, R_6, R_{11} and R_{18}

The reactive power injection in this case is 72.1 KVAR which is equal to that in case 1.1. The similarity is because the PCVC algorithm is used which gives the optimal solution. The minimum bus voltage in the network, i.e. bus R_{11} is considered as one of the measured buses in both the cases and the PCVC aims to get the minimum voltage inside the voltage limits. Although the results are identical, the computational time is much higher in this case. It takes 33ms to compute the PCVC algorithm.

4.7.2.3 Case 3: All the buses in the network

In this case, all the buses in the network are considered as measured buses. Figure 4.34 shows the voltages in all the buses in the network.

As explained above the results are identical to case 2 and case 1.2. The total reactive power injected from the converters is 72.1 KVAR. The difference can be seen in the computational time for the solving the PCVC algorithm. It takes 208ms to compute the PCVC algorithm. This clearly implies that with larger number of buses selected as measured buses, the computational time would increase.

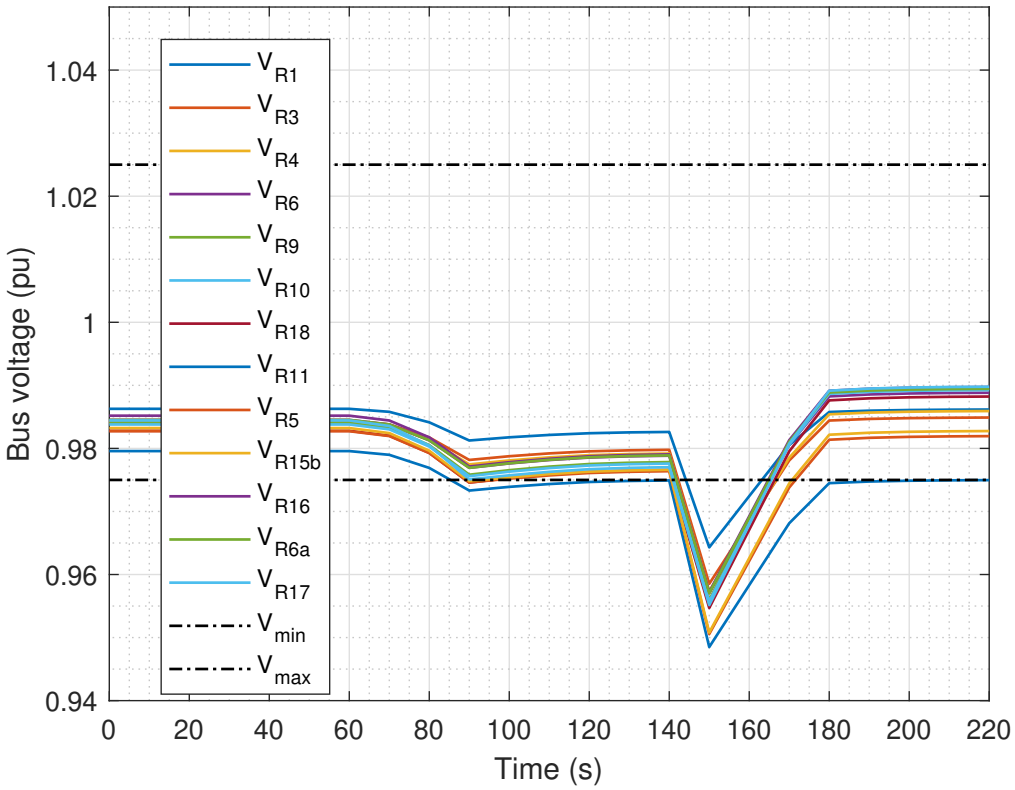

Figure 4.34: All network buses

4.7.2.4 Scenario 2: Discussion

While selecting the number of measured buses, there is a trade off between the optimal control of the network and the computational time of the MPC controller. More measured buses will give higher reliability in case of an unwanted incident like a short circuit or huge increase/ decrease in loads, since it can track the voltages at more number of buses, but will require more computational time to solve the algorithm. Lesser buses will lead to faster solving of MPC optimization but can be less reliable in case of an unwanted sudden incident. Which buses are selected for monitoring also matters as seen in two subcases in Section 4.7.2.1. Table 4.3 gives a case-wise summary for scenario 2.

Scenario	Measured buses	Q injected (KVAR)	Simulation time (s)
Case 1.1	R_{11}	71.2	0.017
Case 1.2	R_6	42.8	0.014
Case 2	R_1, R_6, R_{11} and R_{18}	71.2	0.033
Case 3	All buses in the network	71.2	0.208

Table 4.3: Case wise summary for scenario 2

For two subcases in case 1, case 1.1 utilises more reactive power but ensures that all the bus voltages are in limits while in case 1.2, the measured bus reaches the limits

but due to lesser reactive power injection, other buses end up with lower voltage values. Also, it can be observed that with more number of buses, the computational time increases.

4.7.3 Scenario 3: Effect of weights of the control devices

Weights given to control devices would make an impact on how much reactive power is utilized by the control devices at PV and BESS. The PCVC strategy is used to understand this scenario. The system used for the study has all the parameters similar to the results discussed in section 4.2 and only the weights to the control devices are altered.

For the current system, 4 control devices are available each with a capacity of 24 KVA. The control devices are installed at buses R_{6a}, R_{15b}, R_{16} and R_{17}. The weight vector in the above mathematical model is defined as $\mathbf{R}$ vector and hence can be defined with the weights assigned to each of the control devices as $\mathbf{R} = [\mathbf{R_{R6a}}, \mathbf{R_{R15b}}, \mathbf{R_{R16}}, \mathbf{R_{R17}}]$. To see the impact due to $\mathbf{R}$, only $\mathbf{R_{R15b}}$ is changed and the other 3 have relatively same weights, ie. $\mathbf{R} = [\ 1, \mathbf{R_{R15b}}, 1, 1]$. 3 cases are discussed below with R_{R15b} being given the lowest, equal and highest weights, respectively. The total reactive power consumed by the control device i is mentioned as Q_i from now onwards.

4.7.3.1 Case 1: Low weight to $\mathbf{R_{R15b}}$

like$_{\text{this}}$ In this case a very low relative weight of 0.01 was assigned to the control device at bus R_{15b}. Hence, $\mathbf{R} = [\ 1, 0.01, 1, 1]$. Fig 4.35 describes the voltages at measured buses and the reactive power consumed at 4 control devices. As seen in the figure, the total reactive power consumed at bus R_{15b} is 23.9 KVAR which almost equals the rated capacity of 24 KVAR. The other 3 buses with equal relative weights consume much lesser reactive power of 15.7 KVAR. This shows that the lower weights assigned results in more utilization of reactive power. The explanation for this is that the objective function in (2.1) is a minimization problem and lower weights of control device at bus R_{15b} means the contribution of the reactive power for that device would be higher in the objective function. This leads to lower weights giving higher reactive power utilization.

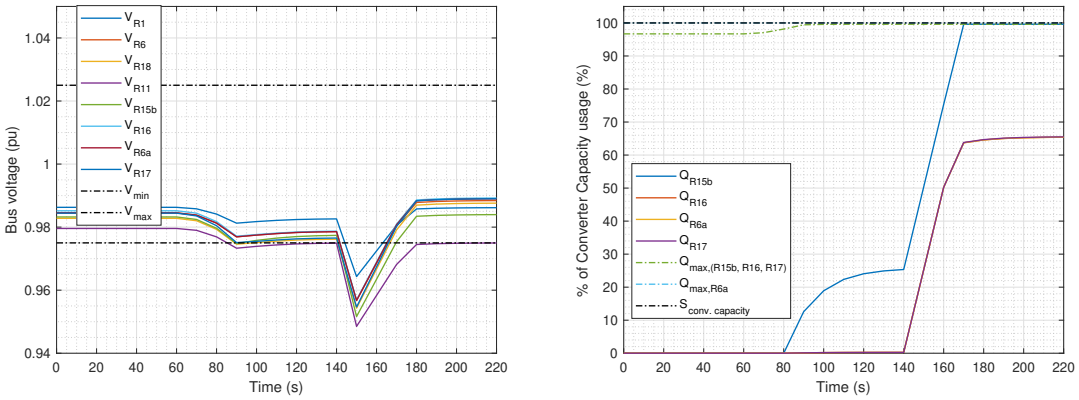

(a) Voltage at measured buses **(b)** Monitored buses

Figure 4.35: Case 1: Very low weights to R_{15b}

4.7.3.2 Case 2: Equal weight to R_{R15b}

In this case control devices at bus R_{15b} is assigned equal weights compared to other 3 devices. This essentially means that $\mathbf{R} = [\ 1,\ 1,\ 1,\ 1]$. Fig 4.36 describes the voltages at measured buses and the reactive power consumed at 4 control devices. As expected, since the relative weights are the same for all the control devices, the reactive power consumption is equal. All of the 4 control devices injects a total of 17.8 KVAR.

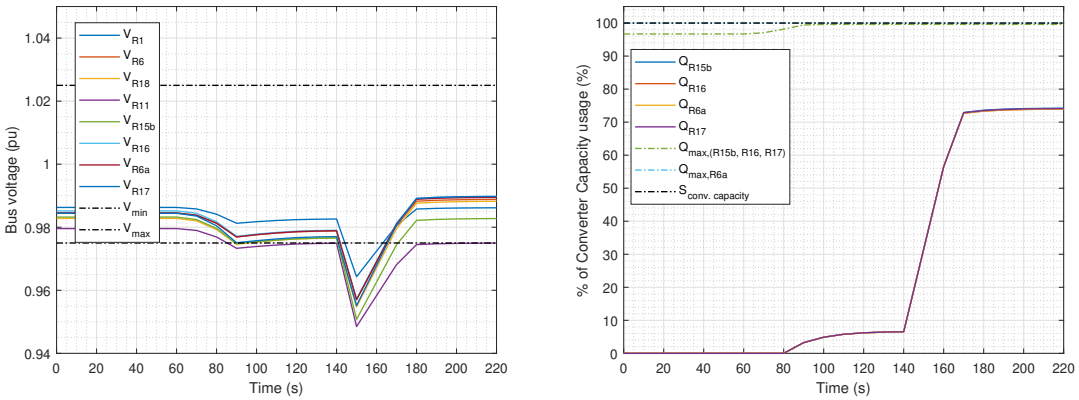

(a) Voltage at measured buses **(b)** Monitored buses

Figure 4.36: Case 2: Equal weights to R_{15b}

4.7.3.3 Case 3: High weight to R_{R15b}

In this case a very high weight of 100 was assigned to the control device at bus R_{15b} which means that $\mathbf{R} = [\ 1,\ 100,\ 1,\ 1]$. Fig 4.37 describes the voltages at measured buses and the reactive power consumed at 4 control devices. The control device at bus R_{15b} injects a total of 12.1 KVAR while the other 3 control devices injects 19.7 KVAR each. As explained above in case 1, because of the minimization problem,

the contribution of higher weight would mean a lower reactive power utilization at that bus which can be seen in the results.

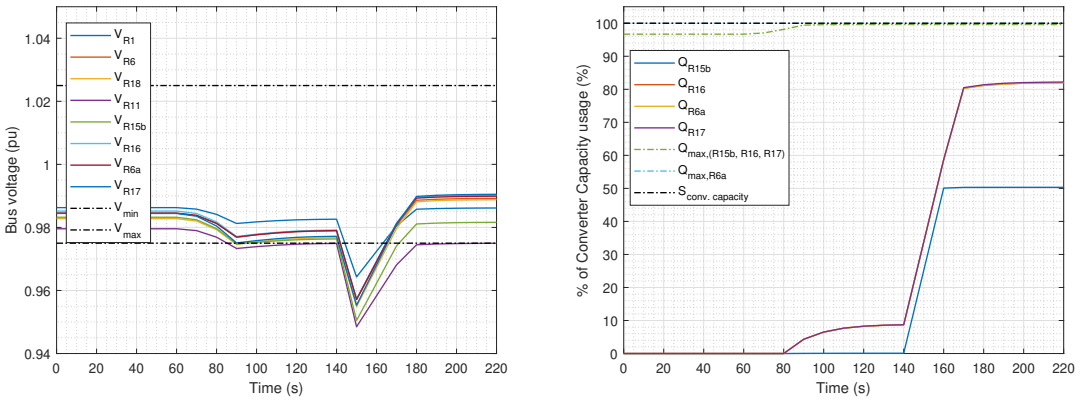

(a) Voltage at measured buses **(b)** Monitored buses

Figure 4.37: Case 3: Very high weights to R_{15b}

4.7.3.4 Scenario 3: Discussion

The weight vector **R** has been varied by keeping 3 of the values same and changing only one weight value at bus $\mathbf{R_{15b}}$. 3 cases were studied with $\mathbf{R_{R15b}}$ being low, equal and high compared to other 3 control devices. It can be observed that when the weight of a certain device is greater than the other devices, it's contribution to the objective function would be lesser in a minimization problem. The results for the above 3 cases can be summarized in the below Table 4.4. All the Q_i are in KVAR. It can be seen that PCVC algorithm consumes the same Q_{total} for all three cases. Only the relative contribution changes based on the relative weights.

R_{R15b}	$\mathbf{Q_{R6a}}$	$\mathbf{Q_{R15b}}$	$\mathbf{Q_{R16}}$	$\mathbf{Q_{R17}}$	$\mathbf{Q_{total}}$
[1, 0.01, 1, 1]	15.7	23.9	15.7	15.7	71.2
[1, 1, 1, 1]	17.8	17.8	17.8	17.8	71.2
[1, 100, 1, 1]	19.7	12.1	19.7	19.7	71.2

Table 4.4: Case wise summary for scenario 3

5
Sustainability aspects

In sustainable development, the needs for the present should be met keeping in mind that it should not hamper the future generation development in meeting their needs. The sustainable development should not adversely affect the ecological, economical and social factors. Each of the three factors has been discussed below from the perspective of the thesis.

5.1 Ecological aspect

Distributed system with large scale integration of DERs would contain PVs and BESS. The mentioned network in the thesis have a large number of solar panels installed. These panels are generally mounted on the roof and hence does not require any extra land space. These solar PVs are clean, renewable source of energy with no harmful emissions.

One disadvantage that could be considered would be the use of lithium ion batteries in the BESS.

5.2 Social aspect

The use of clean renewable sources is encouraged by the society to control the climate change. Using solar PV could save energy bills and also benefit the environment.

5.3 Economical aspect

PV installation could be costly but due to longer life of these panels, the returns are more. Also, by using BESS. the energy could be saved during the hours when the electricity prices are high and can be utilized when these prices reduce leading to a profit. Also, with respect to a model predictive controller, if a DSO is present to operate the distribution system, the system can be better controlled. Adding a price variable into the objective function could increase the profits.

6
Conclusion and future work

6.1 Conclusions

The master thesis investigated different MPC models for the distribution systems with large scale integration of DERs. The different MPC strategies namely, centralised decentralised and distributed were described in detail, theoretically and mathematically. These MPC strategies were compared in terms of the reactive power usage, their performance in the control and the processing times for the algorithm. Later a few scenarios were discussed which described how the change in MPC parameters can have an impact on the system control. The following conclusions can be made for the different MPC strategies:

- Centralized MPC (PCVC) gives a system-wide optimal solution for the voltage regulation but since there is only a single controller for the whole system, the reliability is very low.
- Decentralized MPC strategy (PDVC) lacks communication between different areas and hence there can be excess reactive power usage due to it. It was seen in the results that PDVC was not able to get the measured bus voltages in the voltage limits for one of the buses. This was due to the lack of information sharing between different areas. PDVC has the simplest architecture of all the strategies discussed in the thesis. This strategy can be utilised in the distribution network areas where the localised voltage issues are significant due to large amount of DERs in that particular area.
- Distributed MPC strategies (P-PDiVC and S-PDiVC) gave similar results in terms of processing times and reactive power injection from the controllers. Although P-PDiVC would be preferred since it has simpler architecture compared to S-PDiVC. P-PDiVC gives comparable results to PCVC.

Based on the above discussion it could be said that P-PDiVC would be a recommended strategy as it has comparable results to the optimal PCVC strategy keeping in consideration the design advantage of PDVC.

Parameters for the MPC strategy implemented should be wisely selected as it can affect the system control and stability. Following conclusions can be drawn for changes in parameters:

- The smaller MPC time-step could control the system faster but might require a much better processing device. Since the distributed strategies requires sharing of information between the area optimizers, the time for that should also be considered along with the processing time for the MPC optimization. With a larger time-step, the processing time would not be a problem but in case of a

sudden unfortunate event, it might fail to notice and lead to system instability. Hence a time-step should be selected considering what for the control.

- By altering the number of measured buses, the results could make a huge impact in terms of processing time and system control. With higher number of measured buses selected, the system would be able to monitor more number of buses in the system leading to higher system reliability but at the cost of higher processing time. Selection should be made based on the processing power device available for the control.
- The relative weights to the control devices affects how much each of the devices would be contributing. With higher weights, the contribution of that device decrease in a minimization problem and hence a lesser reactive power utilization.

6.2 Future work

For future work, a suggested enhancement could be varying the control inputs. The thesis focuses on controlling only the reactive power of the DERs. An attempt can be made to implement various control inputs like the tap changer and active power of PV. Additionally see the results for a stronger network would be an interesting case.

Bibliography

[1] Fuel report: International Energy Agency, October 2019, https://www.iea.org/reports/renewables-2019

[2] Renewable Energy Capacity Statistics 2020, IRENA, https://www.irena.org/-/media/Files/IRENA/Agency/Publication/2020/Mar/IRENA_RE_Capacity_Statistics_2020.pdf

[3] Pedro S. Moura and Anıbal T. de Almeida, "Large Scale Integration of Wind Power Generation", Handbook of Power Systems I, M. Panos Pardalos, Steffen Rebennack, F. Mario V. Pereira, and A. Niko Iliadis, Eds., Berlin, Heidelberg: Springer Berlin Heidelberg, 2010, pp. 95–119.

[4] F. Katiraei and J.R. Aguero, "Solar PV Integration Challenges", *IEEE power and energy magazine*, vol. 9, no. 3, 62–71, 2011. doi: 10.1109/MPE.2011.940579.

[5] *VDE-AR-N 4105:2011-08 Power generation systems connected to the low-voltage distribution network - Technical minimum requirements for the connection to and parallel operation with low-voltage distribution networks*. Association for Electrical Electronic & Information Technologies (VDE), 2011.

[6] J. von Appen, M. Braun, T. Stetz, K. Diwold, and D. Geibel, "Time in the Sun: The Challenge of High PV Penetration in the German Electric Grid", *Ieee power and energy magazine*, vol. 11, no. 2, 55–64, Mar. 2013. doi: 10.1109/MPE.2012.2234407.

[7] I. Leisse, O. Samuelsson, and J. Svensson, "Electricity meters for coordinated voltage control in medium voltage networks with wind power", *Innovative Smart Grid Technologies Conference Europe (ISGT Europe), 2010 IEEE PES*, Oct. 2010. doi: 10.1109/ISGTEUROPE.2010.5638977

[8] *Connecting and operating storage units in low voltage networks*. Association for Electrical Electronic & Information Technologies (VDE). Available: https://www.vde.com/en/fnn/documents/fnnconnecting-operating-storage-units-in-lowvoltage-networks2013-06.pdf

[9] James B. Rawlings and Brett T. Stewart, "Coordinating multiple optimization based controllers: New opportunities and challenges", Journal of process control, Selected Papers From Two Joint Conferences: 8th International Symposium on Dynamics and Control of Process Systems and the 10th Conference Applications in Biotechnology, vol. 18, no. 9, 839–845, Oct. 2008. doi: 10.1016/j . jprocont.2008.06.005. [Online]. Available: https://www.sciencedirect.com/science/article/pii/S0959152408001054

[10] T. Stetz, F. Marten, and M. Braun, “Improved Low Voltage Grid-Integration of Photovoltaic Systems in Germany”, *Ieee transactions on sustainable energy*, vol. 4,no. 2, 534–542, Apr. 2013. doi: 10.1109/TSTE.2012.2198925.

[11] G. Valverde and T. Van Cutsem, “Model Predictive Control of Voltages in Active Distribution Networks”, *IEEE transactions on smart grid*, no. 4, Dec. 2013

[12] S. N. Salih and P. Chen, “On Coordinated Control of OLTC and Reactive Power Compensation for Voltage Regulation in Distribution Systems With Wind Power”, *Ieee transactions on power systems*, vol. 31, no. 5, 4026–4035, Sep. 2016. doi:10.1109/TPWRS.2015.2501433.

[13] K. Worthmann, C. M. Kellett, P. Braun, L. Grune, and S. R. Weller, “Distributed and Decentralized Control of Residential Energy Systems Incorporating Battery Storage”, *Ieee transactions on smart grid*, vol. 6, no. 4, 1914–1923, Jul. 2015. doi: 10.1109/TSG.2015.2392081.

[14] Pawan Balram (2016), *On Optimization Based Control of Distributed Energy Resources in Power Systems* (Doctoral dissertation)

[15] MATLAB, Version (r2019a). Natick, Massachusetts: The MathWorks Inc., 2019.

[16] David Sandahl, *Solar PV coupled with electricity storage in Sweden*,Master thesis, Department of Sustainable Energy Systems, Chalmers University of Technology . Available: `https://odr.chalmers.se/bitstream/20.500.12380/257284/1/257284.pdf`

[17] B. Jones-Albertus, "Confronting the Duck Curve: How to Address Over-Generation of Solar Energy" [Online], `https://www.energy.gov/eere/articles/confronting-duck-curve-how-address-over-generation-solar-energy`

[18] International Renewable Energy Agency, ”Battery Storage for Renewables: Market Status and Technology Outlook.” [Online]. Available: `https://www.irena.org/documentdownloads/publications/irena_battery_storage_report_2015.pdf`

[19] Y. Guo, Q. Wu, H. Gao, S. Huang, B. Zhou and C. Li, "Double-Time-Scale Coordinated Voltage Control in Active Distribution Networks Based on MPC," in *IEEE Transactions on Sustainable Energy*, vol. 11, no. 1, pp. 294-303, Jan. 2020, doi: 10.1109/TSTE.2018.2890621.

[20] Jan Marian Maciejowski, *Predictive control: With constraints*. Pearson education, 2002.

[21] Jinfeng Liu, David Mu~noz de la Pe~na, and Panagiotis D. Christofides, “Distributed model predictive control of nonlinear process systems”, en, *Aiche journal*, vol. 55, no. 5, 1171–1184, May 2009. doi: 10.1002/aic.11801. [Online]. Available: `https://aiche.onlinelibrary.wiley.com/doi/abs/10.1002/aic.11801`

[22] Brett T. Stewart and Aswin N. Venkat and James B. Rawlings and Stephen J. Wright and Gabriele Pannocchia, "Cooperative distributed model predictive control", *Systems & Control Letters*, vol. 59, no. 8, 460–469, Aug. 2010. doi: 10.1016/j.sysconle.2010.06.005, `http://www.sciencedirect.com/science/article/pii/S0167691110000691`

[23] SolarPower Europe, ”Global Market Outlook 2018-2022.” [Online]. Available: https://www.solarpowereurope.org/wp-content/uploads/2018/09/Global-Market-Outlook-2018-2022.pdf

[24] J. Lindahl, ”National Survey Report of PV Power Applications in Sweden - 2016.” [Online]. Available: https://iea-pvps.org/?id=93&tx_damfrontend_pi1%5BcatPlus%5D&tx_damfrontend_pi1%5BcatEquals%5D&tx_damfrontend_pi1%5BcatMinus%5D&tx_damfrontend_pi1%5BcatPlus_Rec%5D=57&tx_damfrontend_pi1%5BcatMinus_Rec%5D&tx_damfrontend_pi1%5BtreeID%5D=201&tx_damfrontend_pi1%5Bid%5D=93

[25] Srivastava, A., Steen, D., Le, A. et al (2019), A Congestion Forecast Framework for Distribution Systems with High Penetration of PV and PEVs IEEE PES PowerTech Conference 2019. http://dx.doi.org/10.1109/PTC.2019.8810871

[26] C. S. Cheng and D. Shirmohammadi, "A three-phase power flow method for real-time distribution system analysis," in *IEEE Transactions on Power Systems*, vol. 10, no. 2, pp. 671-679, May 1995, doi: 10.1109/59.387902.

[27] *Benchmark systems for network integration of renewable and distributed energy resources.* CIGRÉ, 2009.

[28] P. Balram, Le Anh Tuan and O. Carlson, "Predictive voltage control of batteries and tap changers in distribution system with photovoltaics," *2016 Power Systems Computation Conference (PSCC), Genoa*, 2016, pp. 1-7, doi: 10.1109/PSCC.2016.7540847.

[29] James B Rawlings and David Q Mayne, *Model predictive control: Theory and design.* Nob Hill Publishing, LLC, 2009.

Appendix

1
Appendix 1

From bus	To bus	Line length (m)	R per unit length[Ω/km]	X per unit length[Ω.km]
R_1	R_3	60	0.190	0.159
R_3	R_4	30	0.190	0.159
R_3	R_{11}	50	0.965	0.805
R_4	R_6	60	0.190	0.159
R_4	R_{15}	45	0.965	0.805
R_6	R_9	90	0.190	0.159
R_6	R_{16}	15	0.965	0.805
R_6	R_{6a}	10	0.965	0.805
R_9	R_{10}	30	0.190	0.159
R_9	R_{17}	50	0.965	0.805
R_{10}	R_{18}	30	0.965	0.805
R_{15}	R_{15b}	10	0.965	0.805

Table 1.1: Line data for the network in Figure 3.1